Ocean Conditions and the Intensification of Three Major Atlantic Hurricanes in 2017

RICARDO DOMINGUES,[a,b] MATTHIEU LE HÉNAFF,[a,b] GEORGE HALLIWELL,[a,b] JUN A. ZHANG,[a,b] FRANCIS BRINGAS,[b] PATRICIA CHARDON,[c] HYUN-SOOK KIM,[b] JULIO MORELL,[c] AND GUSTAVO GONI[b]

[a] *University of Miami, Cooperative Institute for Marine and Atmospheric Studies, Miami, Florida*
[b] *National Oceanic and Atmospheric Administration, Atlantic Oceanographic and Meteorological Laboratory, Miami, Florida*
[c] *University of Puerto Rico at Mayaguez, Mayaguez, Puerto Rico*

(Manuscript received 31 March 2020, in final form 25 November 2020)

ABSTRACT: Major Atlantic hurricanes Irma, Jose, and Maria of 2017 reached their peak intensity in September while traveling over the tropical North Atlantic Ocean and Caribbean Sea, where both atmospheric and ocean conditions were favorable for intensification. In situ and satellite ocean observations revealed that conditions in these areas exhibited (i) sea surface temperatures above 28°C, (ii) upper-ocean heat content above 60 kJ cm^{-2}, and (iii) the presence of low-salinity barrier layers associated with a larger-than-usual extension of the Amazon and Orinoco riverine plumes. Proof-of-concept coupled ocean–hurricane numerical model experiments demonstrated that the accurate representation of such ocean conditions led to an improvement in the simulated intensity of Hurricane Maria for the 3 days preceding landfall in Puerto Rico, when compared to an experiment without the assimilation of ocean observations. Without the assimilation of ocean observations, upper-ocean thermal conditions were generally colder than observations, resulting in reduced air–sea enthalpy fluxes—enthalpy fluxes are more realistically simulated when the upper-ocean temperature and salinity structure is better represented in the model. Our results further showed that different components of the ocean observing system provide valuable information in support of improved TC simulations, and that assimilation of underwater glider observations alone enabled the largest improvement over the 24 h time frame before landfall. Our results, therefore, indicated that ocean conditions were relevant for more realistically simulating Hurricane Maria's intensity. However, further research based on a comprehensive set of hurricane cases is required to confirm robust improvements to forecast systems.

KEYWORDS: Hurricanes/typhoons; Air-sea interaction; In situ oceanic observations; Coupled models; Data assimilation

1. Introduction

Coupled ocean–atmosphere prediction models provide critical information to hurricane forecasters tasked with providing the public with accurate forecasts. Recent studies using ocean profilers and satellite-derived data and products have demonstrated that ocean conditions can play a role on tropical cyclone (TC) intensity (e.g., Shay et al. 2000; Shay and Jacob 2006; Shay and Uhlhorn 2008; Mainelli et al. 2008; Goni et al. 2009; Seroka et al. 2017; Goni et al. 2017; Goni and Domingues 2019). Collectively, these studies demonstrated that, under a favorable atmospheric environment, TC intensity evolution can be influenced by the temperature and salinity vertical structure, including the upper-ocean heat content [represented by the tropical cyclone heat potential (TCHP)] associated with oceanic eddies and boundary currents. The genesis and intensification of hurricanes is often associated with TCs moving over oceanic areas that exhibit one or more of three distinctive conditions: 1) sea surface temperatures (SSTs) above 26°C (Leipper and Volgenau 1972; Dare and McBride 2011); 2) TCHP values greater than 50 kJ cm^{-2} (e.g., Shay et al. 2000; Mainelli et al. 2008; Goni et al. 2009); and 3) low sea surface salinity (SSS) values that can produce barrier layer conditions. When two or more of these parameters overlap, preexisting upper-ocean conditions will generally sustain SSTs larger than 26°C throughout the passage of hurricanes, and may help maintain its intensity and potentially sustain further intensification. Ocean barrier layers, for example, arise because low SSS defines an enhanced vertical density gradient in the upper-ocean that may suppress the hurricane-forced turbulent mixing (see Rudzin et al. 2018), and with that help maintain warm SSTs throughout the storm. Low SSS barrier layer effects on TCs have been recognized in the North Atlantic (e.g., Ffield 2007; Balaguru et al. 2012; Reul et al. 2014a; Domingues et al. 2015; Androulidakis et al. 2016), north Indian Ocean (e.g., Vissa et al. 2013), and western Pacific basins (e.g., Wang et al. 2011).

Operational systems used for hurricane forecasting in the North Atlantic basin often employ ocean fields based on subsets of NOAA's global Real Time Ocean Forecast System (RTOFS), which runs daily to produce 2 days of nowcasts based on initial conditions provided by The Naval Oceanographic Office using the Navy Coupled Ocean Data Assimilation system (NCODA). NCODA assimilates all real-time ocean observations [e.g., observations from satellite-altimetry, Argo floats, expendable bathythermographs (XBTs), underwater gliders] available within the Global Telecommunications Systems using a 3D multivariate data assimilation methodology (Cummings 2005). With this framework, ocean observations used in operational forecasts are at best 2 days old, which likely provide enough

Supplemental information related to this paper is available at the Journals Online website: https://doi.org/10.1175/MWR-D-20-0100.s1.

Corresponding author: Ricardo Domingues, ricardo.domingues@noaa.gov

DOI: 10.1175/MWR-D-20-0100.1

accuracy to constrain the ocean mesoscale and prestorm vertical conditions, such as those conditions observed in 2017. Recent studies have demonstrated that accurate initialization of the ocean component in coupled modeling systems achieved through ocean data assimilation can, in fact, potentially help to more realistically simulate hurricane intensification (e.g., Dong et al. 2017; Mogensen et al. 2017).

While near real-time ocean observations, such as those from satellite-altimetry, underwater gliders, and Argo floats, are already routinely used within operational forecasts, assessing their specific value/contribution toward better forecasts is important to support cost-effective improvements in the forecast systems. The state of the art approach of Observing System Experiments (OSE, and Observing System Simulation Experiments–OSSE) provides a valuable tool to evaluate the value of specific components of the ocean observing system for operational applications (e.g., Oke et al. 2009, 2015; Fujii et al. 2019). Unfortunately, only limited ocean OSE research has been conducted to date to document the sensitivity of coupled ocean–hurricane model intensity errors to the accuracy of ocean model initialization. The importance of reducing initialization errors was recently demonstrated by Dong et al. (2017), who documented a 50% improvement in the simulated intensity of Hurricane Gonzalo (2014) when ocean observations were assimilated, compared to an unconstrained ocean model simulation (i.e., no data assimilation). However, findings from Dong et al. (2017) remain to be evaluated in other case studies, as the number of studies quantifying the potential impact of ocean conditions on hurricane intensification using ocean–hurricane coupled models is still very limited (see Domingues et al. 2019).

The 2017 Atlantic hurricane season produced a suitable scenario for assessing the impact of the ocean on TC intensification, since it featured 18 named storms, from which six became major hurricanes (>category 3 on the Saffir–Simpson wind scale; Schott et al. 2019) with winds stronger than 96 kt (1 kt $\approx$ 0.51 m s^{-1}) (National Hurricane Center 2017). This activity was above normal, as a typical season exhibits the development of 12 named TCs, with six TCs becoming hurricanes and two TCs becoming major hurricanes (e.g., Landsea 1993). Among the major hurricanes of 2017, Hurricanes Irma and Maria (studied here) were among the top five costliest Atlantic hurricanes in history (through 2019). Hurricane Irma started experiencing initial periods of rapid intensification in the eastern Atlantic Ocean, and later reached its peak intensity while traveling over areas in the tropical North Atlantic Ocean and Caribbean Sea within 12°–20°N, 55°–65°W (Fig. 1), where both major Hurricanes Jose and Maria also intensified to their peak intensity 3 days and 12 days later, respectively. These areas exhibited a favorable atmospheric environment for TC intensification (Landsea 2017; Berg 2017, 2018; Cangialosi et al. 2018; Pasch et al. 2019), and a previous study pointed out that the large SSTs anomalies present in these areas were a key precursor for supporting their rapid intensification (Murakami et al. 2018). In addition, the area where they intensified to their peak intensity was associated with additional sufficiently favorable oceanic conditions for TC intensification, jointly characterized by SSTs above 26°C, TCHP values greater than 50 kJ cm^{-2}, and SSS below 35, which may have played a secondary role in further

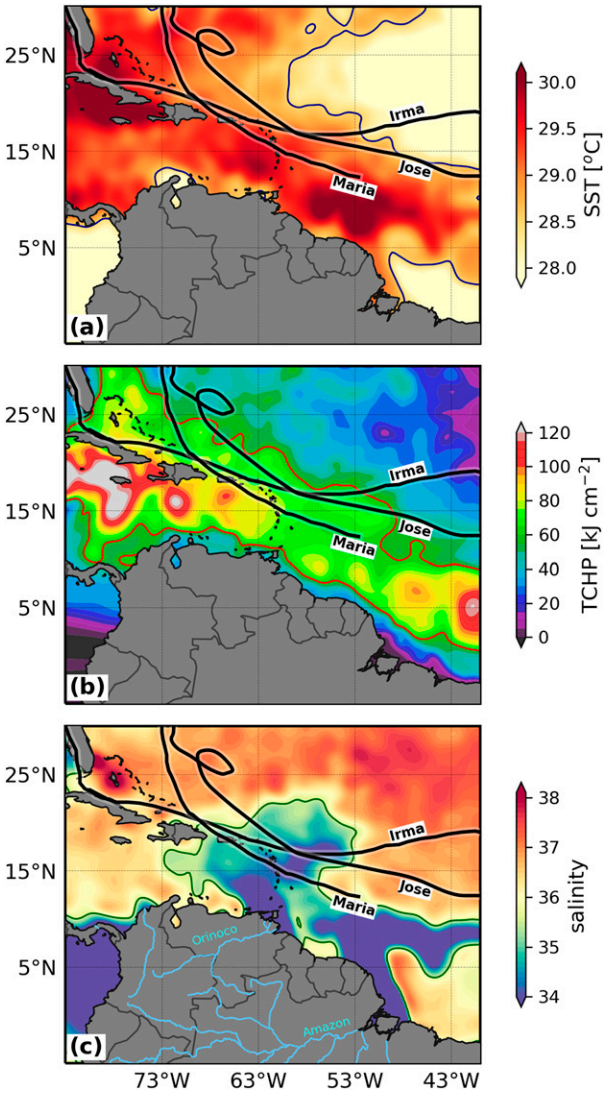

FIG. 1. Ocean conditions on 28 Aug 2017 in the Caribbean Sea and tropical North Atlantic Ocean in terms of (a) SST, (b) TCHP, and (c) satellite-derived sea surface salinity (SSS). Solid lines in (a)–(c) show the 28°C, the 60 kJ cm^{-2}, and the 35 salinity contours, respectively.

contributing with their intensification (for a brief synoptic history of these hurricanes, please refer to the online supplemental material). These three storms caused extensive damage in the Lesser Antilles, Puerto Rico, Cuba, and the continental United States, with Hurricane Maria also causing thousands of fatalities in Puerto Rico (Santos-Burgoa et al. 2018). Therefore, detailed analysis of the conditions that enabled them to become major hurricanes may prove helpful to further understand the impact of the ocean on TC intensification.

The main objectives of this study are, therefore, to 1) assess the ocean conditions before, during, and after the passage of the 2017 major hurricanes Irma, Jose, and Maria; 2) evaluate the impact of ocean data assimilation on the representation of such ocean conditions within a coupled ocean–hurricane model; and

TABLE 1. Summary of the interaction of Hurricanes Irma, Jose, and Maria with three underwater gliders. Winds at the glider location are derived from Air Force Stepped Frequency Microwave Radiometer aircraft surveys. Aircraft mission number and start time are shown in the last column.

Hurricane	Glider	Time of closest hurricane approach	Min distance to hurricane (closest approach)	Winds at the location of the glider
Irma	SG635	0310 UTC 7 Sep 2017	190 km	43–52 kt (22–27 m s^{-1}); flight mission 15, 0604 UTC 7 Sep 2017
Jose	SG635	1440 UTC 10 Sep 2017	115 km	37–41 kt (19–21 m s^{-1}); flight mission 04, 0243 UTC 10 Sep 2017
Maria	SG610	1710 UTC 20 Sep 2017	170 km	41–47 kt (21–24 m s^{-1}); flight mission 07, 0837 UTC 20 Sep 2017
	SG630	0858 UTC 20 Sep 2017	232 km	—

3) demonstrate the potential impact of observed ocean conditions on the intensity of hurricane Maria. To accomplish objective 1), ocean conditions available in 2017 before the passage of these hurricanes are described and compared against historical/average conditions in section 2. To accomplish objective 2), we ran an experimental coupled atmospheric–ocean model maintained by NOAA/AOML (described in section 3) to assess the impact of ocean conditions on Hurricane Maria based on proof-of-concept experiments. In the interest of brevity, we focus our coupled-modeling experiments on the case of Hurricane Maria, and carry out a detailed assessment of the impact of ocean conditions. In section 4 we discuss how our results relate to and complement previous efforts aimed at demonstrating the impact of the ocean on hurricane intensification.

2. Ocean conditions during the 2017 Atlantic hurricane season

a. Data

We used satellite and in situ ocean observations collected in the areas where Hurricanes Irma, Jose, and Maria traveled and intensified to characterize the ocean conditions before, during, and after their passage. Satellite-derived SST, TCHP, and SSS data are used here to assess baseline ocean conditions during August 2017 before the passage of these three hurricanes and how these conditions differed from average conditions throughout the time period of 1993–2017. We note that, due to cloud cover and instrument biases, satellite-derived SST fields may often include errors of the order of a few decimal degrees Celsius. However, the NOAA High-Resolution Optimally Interpolated SST, which is used in our study, employs an operational bias correction based on available in situ observations that minimizes such large-scale biases (Reynolds et al. 2002).

To complement the SSS data, we also used satellite-derived chlorophyll-a data to identify the extension of the Amazon and Orinoco riverine plumes. These plumes are rich in nutrients that favor phytoplankton production (e.g., Goes et al. 2014), and are generally associated with high chlorophyll-a values. In fact, both satellite-derived chlorophyll-a estimates and SSS estimates showed a significant correlation with in situ SSS observations from underwater gliders (Figs. S1 and S2 in the online supplemental material), enabling chlorophyll-a data to be used as a proxy to characterize the presence of freshwater in the region. We also used sea surface height (SSH) observations from satellite altimetry that were assimilated into an ocean model for initializing our coupled ocean–hurricane model experiments (see section 3a).

In addition to satellite observations, various platforms also provided in situ observations in the tropical North Atlantic Ocean during the study period, including moorings, underwater gliders, XBT transects, surface drifters, and profiling floats (Argo and Alamo). Most of these observing platforms belong to the sustained ocean observing system and are carried out in support of long-term climate monitoring (Legler et al. 2015). However, sustained ocean observations to specifically support hurricane studies and forecasts were not implemented until 2014 (Domingues et al. 2019). Since then, pilot networks of underwater gliders have been deployed in the Caribbean Sea and North Atlantic Ocean specifically to collect observations from areas where hurricanes commonly travel and intensify (e.g., Domingues et al. 2015; Miles et al. 2015; Seroka et al. 2017). During the 2017 Atlantic hurricane season, three Seagliders (Eriksen et al. 2001, hereafter referred to as underwater gliders) deployed and operated by NOAA surveyed ocean areas where Irma, Jose, and Maria traveled, collecting more than 120 temperature and salinity profiles in the vicinity of their tracks (Table 1). Underwater gliders profiled between the sea surface and the 500 m depth every ~2 h, producing two profiles (e.g., during the dive and climb), and moving up to 3 km horizontally around a fixed target during each dive cycle. All glider temperature and salinity profiles were corrected for sensor lags (Morison et al. 1994) and thermal inertia effects (Lueck and Picklo 1990), and quality controlled based on gross-range tests, spike detection, vertical gradients checks, and comparison to climatological temperature and salinity from the World Ocean Atlas 2013 (Locarnini et al. 2013; Zweng et al. 2013). These in situ ocean observations were used in two ways: 1) glider data assessed prestorm conditions and the upper-ocean response to Hurricanes Irma, Jose, and Maria (section 3c); and 2) temperature and salinity profiles from profiling floats (4595 profiles, Fig. S3) and underwater gliders (4200 profiles, Fig. 2b) were assimilated into an ocean model (section 3).

b. Baseline ocean conditions for August 2017

The ocean conditions present in the Caribbean Sea and tropical North Atlantic in late-August 2017 prior to the passage of Hurricanes Irma, Jose, and Maria in September 2017 are referred to as baseline conditions, whereas prestorm conditions

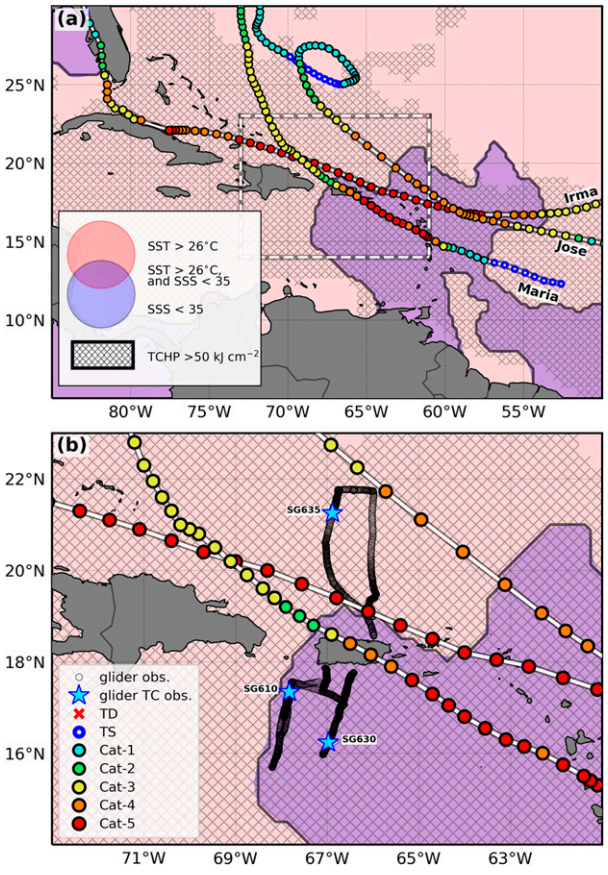

FIG. 2. (a) Tracks of major Atlantic Hurricanes Irma, Jose, and Maria, with their respective intensities. (b) Locations sampled by three NOAA hurricane underwater gliders during the 2017 Atlantic hurricane season, with their locations at the time of hurricane's closest approach (see Table 1). Pink areas indicate locations with SSTs warmer than 26°C. Purple areas indicate locations where SSTs are warmer than 26°C and SSS less than 35. Hatched areas correspond to locations where TCHP is greater than 50 kJ cm^{-2}.

refer to the ocean conditions just before (typically 24 h) the passage of each storm (section 2c). Baseline conditions on 28 August 2017 (Fig. 1) were characterized by: (i) warm SSTs with values ranging from 28° to 30°C (Fig. 1a); large values of TCHP (>60 kJ cm^{-2}), reaching 80–100 kJ cm^{-2} in the Caribbean Sea (Fig. 1b); and low SSS (<35) with values as low as 34.5 in the Caribbean Sea, associated with the Amazon and Orinoco riverine plumes (Fig. 1c). Figure 2 illustrates how Hurricanes Irma, Jose, and Maria intensified to their respective maximum intensity while traveling over areas that included these three overlapping ocean conditions (Fig. 2a). These areas were surveyed by the three underwater gliders operated by NOAA (Fig. 2b), which confirmed the favorable upper-ocean conditions identified by satellite data and enabled a detailed assessment of the upper-ocean response forced by Hurricanes Irma, Jose, and Maria (see section 2c).

Analysis of satellite-derived historical ocean conditions in the Caribbean Sea and tropical North Atlantic Ocean during 1993–2016 showed that the baseline values observed in August 2017 tended to be more favorable than normal for TC intensification (Fig. 3). First, SST values were approximately 0.4°C warmer than the 1993–2016 August mean in the Caribbean Sea and 0.2°C warmer in the tropical North Atlantic Ocean portion of the study area (Figs. 3a,b). These warm SST anomalies were acknowledged by Murakami et al. (2018) as a key factor supporting the major hurricane activity observed in 2017. In addition, the average TCHP anomaly values during August 2017 were also larger than the 1993–2016 August mean by approximately 10 kJ cm^{-2} in the Caribbean Sea, although they were close to average conditions in the tropical North Atlantic Ocean portion of our study area (Figs. 3c,d).

Because satellite SSS data were unavailable before 2010, we used MODIS-*Aqua* chlorophyll-a data, available beginning in 2002, to characterize freshwater inputs from rivers in the region. Based on the significant ($p < 0.05$) relationships between SSS and chlorophyll-a in the region (Fig. S1), monthly averaged chlorophyll-a data in August 2017 indicated that there was lower salinity water in the Caribbean Sea compared to the climatological August conditions (Fig. 3e). In fact, observations from underwater gliders further confirmed that upper-ocean salinity was lower than normal (section 2c). In the tropical North Atlantic Ocean portion of our study area, values were close to average (Fig. 3f). In August 2017, freshwater riverine plumes associated with the Amazon and Orinoco Rivers occupied a large area extending from the Amazon River mouth to areas northeast of the Lesser Antilles and into the Caribbean Sea (Fig. 1c). The analysis of monthly chlorophyll-a composites and altimetry-derived geostrophic velocity fields from March through August 2017 indicated that the establishment of this extended low-salinity area observed in August was likely due to the entrainment of low-salinity and chlorophyll-rich riverine waters by mesoscale ocean eddies from April through June 2017 (Fig. S2b–d), which also coincided with the months of peak discharge by these rivers (e.g., Smith and Demaster 1996; Reul et al. 2014b). Entrainment of the Amazon–Orinoco waters has been recognized as a potential source of interannual hurricane activity in the Atlantic (Ffield 2007).

c. *Prestorm conditions and ocean response to major 2017 hurricanes*

We assessed prestorm ocean conditions, typically 24 h before the passage of a given storm, and the ocean response forced by Hurricanes Irma, Jose, and Maria. The analysis focused on underwater glider observations (Fig. 2b), which surveyed areas in the Caribbean Sea and tropical North Atlantic Ocean off the coast of Puerto Rico, where satellite observations have shown that SSTs were larger than 28°C, TCHP values larger than 60 kJ cm^{-2}, and SSSs were below 35. These underwater glider observations are analyzed as a reasonable representation of conditions for neighboring areas that exhibited these three satellite-derived ocean conditions (e.g., Fig. 2a), also where the three hurricanes reached their peak intensity. However, it should be acknowledged that gliders sampled areas located in the outskirts of these three hurricanes (Table 1), and that after reaching their peak intensity, the three systems underwent weakening as they traveled in the proximity of the gliders (see Cangialosi et al. 2018; Berg 2018; Pasch et al. 2019).

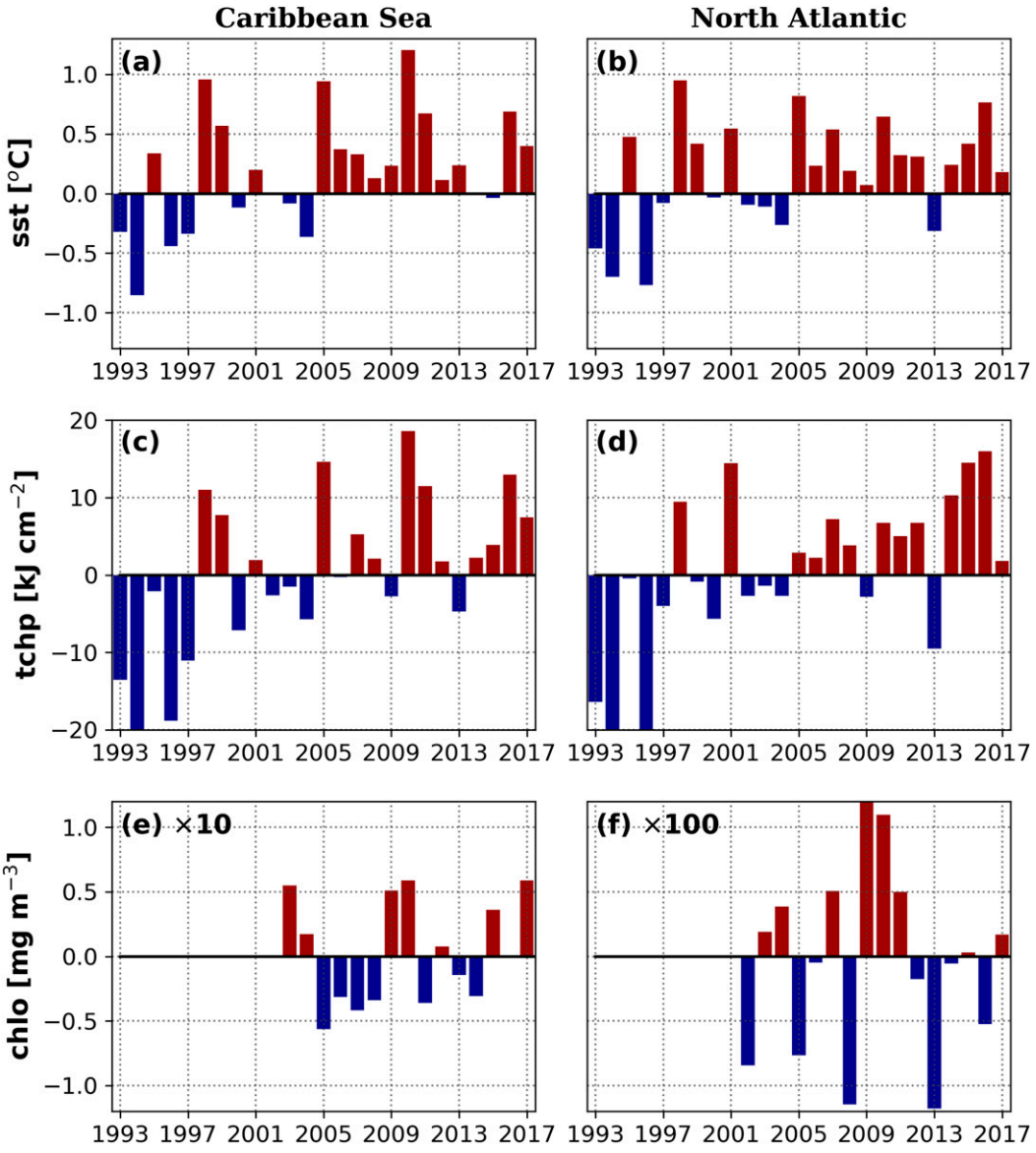

FIG. 3. Anomalies, with respect to mean August ocean conditions during 1993–2017 (2002–17 for chlorophyll), in terms of (a),(b) SST; (c),(d) TCHP; and (e),(f) surface chlorophyll-a for (left) the Caribbean Sea and (right) the tropical North Atlantic Ocean. The satellite-derived time series displayed are of averaged August anomalies within 19°–22°N, 65.5°–67°W in the tropical North Atlantic Ocean and 15°–18°N, 66.5°–68.5°W in the Caribbean Sea.

Hurricane Irma traveled within 190 km of glider SG635 as a category-5 TC at 0310 UTC 7 September 2017 (Table 1), with the glider located in the stronger part of the storm to the right of the track (Fig. 2b). Irma reached a peak intensity of 155 kt (287 km h^{-1}) with a minimum pressure of 914 hPa. This made Irma the most intense TC globally in 2017 during the few days prior to passing close to the glider when the storm moved over especially warm and freshwater (Fig. 2). Glider observations revealed that Irma traveled over upper-ocean temperature conditions characterized by an isothermal layer in the upper 45 m associated with SSTs above 29°C (red line, Fig. 4a), which were approximately 1°C higher than the climatological value at this location (green line, Fig. 4a). The prestorm salinity profile revealed isohaline conditions in the upper 40 m (red line, Fig. 4b) that were approximately 0.7 fresher than the mean August conditions (green line, Fig. 4b). This halocline defined a prestorm barrier layer ~10 m thick (red line, Fig. 5a), which was calculated as the difference between the surface isothermal layer depth defined using a threshold of 0.5°C, and the mixed layer depth defined using a density threshold of 0.2 kg cm^{-3} (see Balaguru et al. 2012).

Air Force Stepped Frequency Microwave Radiometer (SFMR) wind observations from mission 15 starting at 0604 UTC 7 September 2017 indicated that the surface wind speed at the

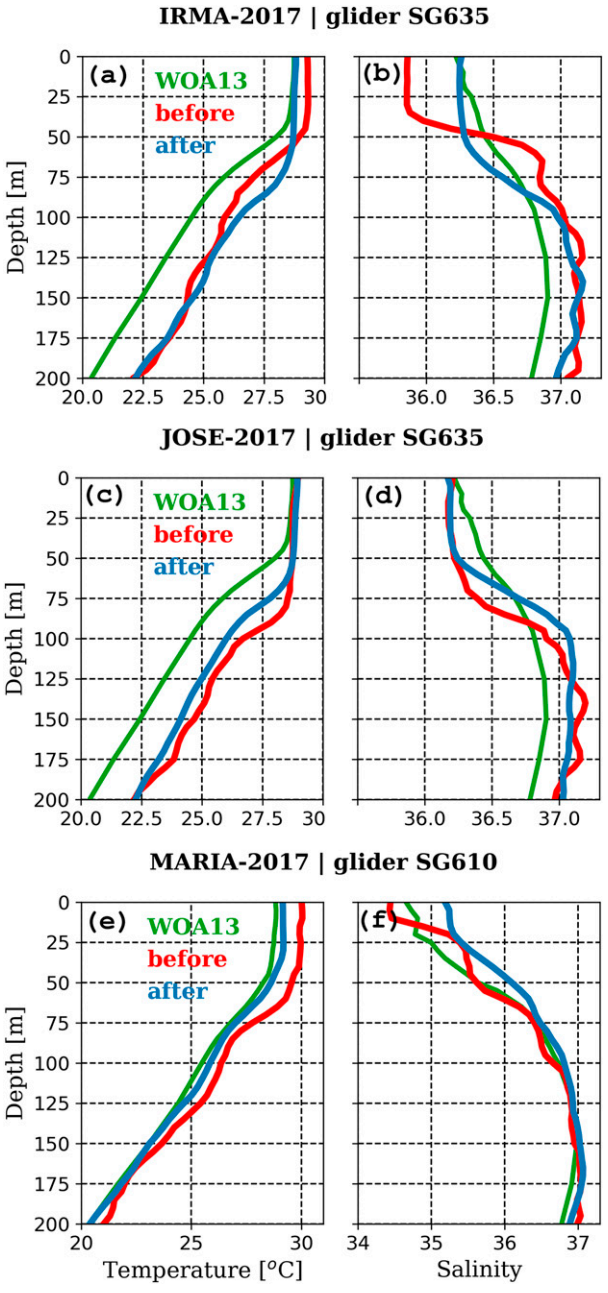

FIG. 4. Temperature and salinity profiles sampled by three underwater gliders (SG610, SG630, and SG635; see Fig. 2b) before (red lines) and after (blue lines) the passage of hurricanes (a),(b) Irma, (c),(d) Jose, and (e),(h) Maria. The climatological August profiles from the World Ocean Atlas (WOA) 2013 are shown (green lines) for comparison purposes.

location of glider SG635 when Irma passed ranged between 43 and 52 kt, based on radial distance (22–27 m s^{-1}, Table 1, Fig. S4). As Irma approached the location of the glider, these tropical storm winds caused the following: 1) the partial erosion of the initial stratification, with the buoyancy frequency dropping from $\sim 10 \times 10^{-4}\,s^{-1}$ before the hurricane to $4 \times 10^{-4}\,s^{-1}$ within the first 24 h after the storm; and 2) a deepening of the mixed layer, which increased from 45 m before the storm to ~75 m in the 24 h after Irma's passage (Fig. 5c). Hurricane-forced mixing caused limited SST cooling of 0.7°C within the 24 h following Irma (Figs. 5b,d). The preexisting barrier layer conditions in this location likely contributed to partially suppressing hurricane-induced SST cooling, as observed during Hurricane Gonzalo in 2014 (Domingues et al. 2015). With this, SSTs were consistently larger than 28°C in the location sampled by glider SG635 throughout the passage of Irma.

A few days later (and at times as a category-4 TC), Hurricane Jose passed over the ocean wake produced by Irma (Fig. 2a). Jose passed within approximately 115 km of the location of glider SG635 (Table 1), which had remained stationed at the same location since before the passage of Irma (Fig. 2b). Glider observations revealed that Jose experienced a well-mixed and slightly colder upper ocean, with SSTs of ~28°C due to the wake left by Hurricane Irma (Fig. 4c). The base of the mixed layer prior to the arrival of Hurricane Jose was located at approximately 80 m depth, as it was previously further mixed by Hurricane Irma. The temporary shoaling of the mixed layer depth prior to Jose (Fig. 5e) depicted one of the signatures of the strong and well-defined internal waves that developed in the wake of Irma and that were later reinforced by Jose. The signature of these waves appeared as oscillations in the base of the mixed layer and upper thermocline with a periodicity of approximately 36 h (Figs. 5e,f). Note that the base of the mixed layer shoaled during the 24 h before Jose (Fig. 5e) and then quickly deepened during the following 0–12 h, becoming shallower once again at the 12–24 h interval. This pattern repeated itself for days beyond the 72 h shown in Fig. 5. Below the mixed layer, strong thermocline oscillations indicative of near-inertial waves were observed at the glider location in response to Hurricanes Irma and Jose (Fig. 5f). While internal waves were one of the main responses observed during Hurricane Jose, the storm did not significantly cool the mixed layer compared to Irma due to the larger thermal inertia associated with the thicker initial mixed layer and because of weaker forcing (Jose's wind field was both smaller and weaker than Irma). In addition, glider SG635 was also positioned to the left of Jose's track, which is understood as the weaker side of Northern Hemisphere TCs, and hence less storm-induced mixing was expected. Compared to Irma, the location surveyed by glider SG635 also experienced tropical storm conditions during Jose, with surface winds ranging between 37 and 41 kt (19–21 m s^{-1}, Table 1, Fig. S4). As Hurricane Jose traveled in the proximity of glider SG635, its intensity declined from category 4 to category 3 (Fig. 2b), which was primarily attributed to the increasing atmospheric shear in this location and an eyewall replacement cycle (Berg 2018). It is likely, however, that the relatively cooler initial ocean conditions experienced by Hurricane Jose in this location compared to Hurricane Irma played a secondary role in further contributing to its weakening. These results are consistent with a previous study (Balaguru et al. 2014) that reported on how cyclone-to-cyclone interactions may help suppress further TC intensification.

Hurricane Maria entered the Caribbean Sea on September 19 following landfall in Dominica, where the storm peaked in

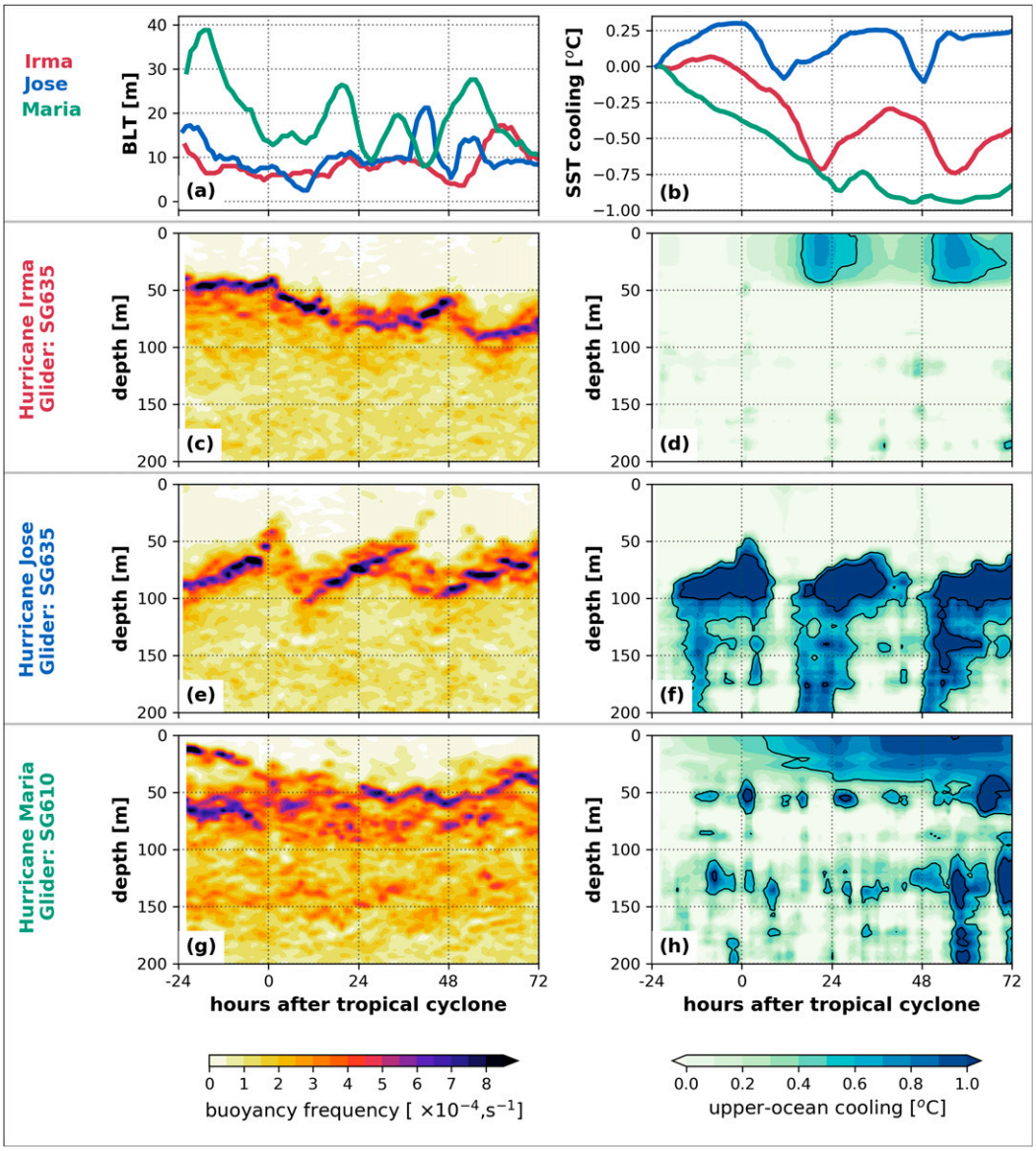

FIG. 5. Prestorm conditions and the upper-ocean response to Hurricanes Irma, Jose, and Maria. (a) Barrier layer thickness sampled by underwater gliders (see Table 1) before, during, and after the passage of the hurricanes. (b) SST cooling sampled by underwater gliders in response to the passage of the hurricanes. (c),(e),(g) Subsurface buoyancy frequency and (d),(f),(h) upper-ocean cooling due to Hurricanes Irma, Jose, and Maria, respectively. Warming anomalies due to mixing below the mixed layer are omitted from (d), (f), and (h) for display purposes. Contours in (d), (f), and (h) are every 0.5°C. The zero hour on the *x* axis indicates the time of closest TC approach from each glider, as described in Table 1.

intensity with maximum sustained winds of 150 kt (280 km h^{-1}). Shortly thereafter, Maria traveled within 232 km of glider SG630 and within 170 km of glider SG610 (Table 1, Fig. 2b). Pre-Maria ocean conditions at the location of glider SG610 were characterized by a thick, warm upper layer with temperatures of ~30°C extending to a depth of approximately 45 m and fresh salinity values of ~34.5 between the surface and 15 m depth (red line, Figs. 4e,f). These conditions were warmer and fresher than climatological values in the area (green line, Figs. 4e,f) and characterized by a thick barrier layer of approximately 30 m at the location of glider SG610 (green line, Fig. 5a). As Maria approached Puerto Rico and the gliders, the stratification (Fig. 5g) and barrier layer (green line, Fig. 5a) were partially eroded by tropical storm wind conditions (41–47 kt) in the location of glider SG610 (Table 1), with the barrier layer reaching its minimum thickness of 15 m within the 24 h preceding the storm's passage. Within 24 h after Maria's closest approach, upper-ocean cooling amounted to 0.8°C, indicating that Maria consistently experienced SSTs above 29°C in the region close to glider SG610. Observations suggest that

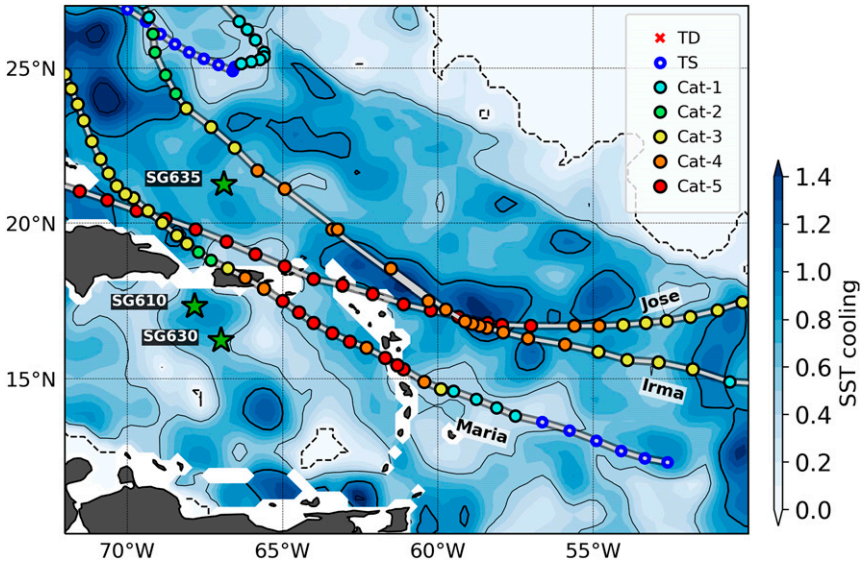

FIG. 6. Satellite-derived SST cooling composite following the passage of 2017 Hurricanes Irma, Jose, and Maria, calculated as described in the text. The 0°C cooling isotherm is depicted by the dashed line, while the thick black line depicts 1°C. Thin contours are every 0.5°C.

turbulent-mixing likely played a dominant role in the SST cooling during the first 24 h following the closest approach of Maria, which is evidenced by the absence of cooling anomalies below the base of the mixed layer during that time-period. During the 24–48 h following the passage of Maria, periodic oscillations in the barrier layer thickness (green line, Fig. 5a) suggested the development of internal waves. In addition, cooling of the entire water column between 48 and 72 h after Maria's passage (Fig. 4e) suggested the development of an upwelling anomaly that likely contributed to cooling SSTs further at the location of glider SG610. The development of an upwelling anomaly in this location is consistent with Maria's wind patterns carrying ocean waters offshore from Puerto Rico (Fig. 2a). The presence of a 30 m thick barrier layer in this location likely helped reduce the wind-driven cooling through turbulent mixing within ±12 h of Maria's passage.

Underwater glider observations indicated that upper-ocean cooling linked with Irma, Jose, and Maria was generally below 1°C at the location of the gliders. However, as described above, gliders sampled the outskirts of these three hurricanes and likely underestimated the potential hurricane-forced cooling. To obtain an improved overview and spatial distribution of the potential hurricane-forced cooling, including areas that were directly exposed to the eyewall, we expand our analysis using satellite-derived data. To accomplish this, an SST cooling composite (Fig. 6) following the passage of Hurricanes Irma, Jose, Maria is calculated as follows: at each grid point, the maximum SST cooling among the three hurricanes is displayed, with the individual storm-induced cooling calculated using SST fields from 9 September 2017 minus 5 September 2017 for Irma; 12 September 2017 minus 8 September 2017 for Jose; and 22 September 2017 minus 18 September 2017 for Maria. This SST-cooling composite (Fig. 6) shows that, in fact, maximum SST-cooling was generally under 1°C in most areas where these hurricanes traveled, with the exception of areas east of the Leeward Islands, where SST cooling larger than 1°C was forced on the right side of Irma. Therefore, although the glider observations captured the ocean response to tropical storm intensity winds in the outer core of these hurricanes, satellite-derived observations revealed that cooling of similar magnitude was also observed in areas directly where the eye passed, and that the three storms consistently experienced SSTs larger than 28°C throughout their passage.

3. Impact of ocean conditions on Hurricane Maria: Proof-of-concept ocean–hurricane coupled experiments

Major hurricanes Irma, Jose, and Maria reached their peak intensity in the western part of the North Atlantic basin, where a favorable atmospheric environment for intensification existed associated with sufficiently favorable ocean conditions revealed by satellite and glider observations. Irma started experiencing rapid intensification far in the eastern Atlantic, and reached these areas already as a category-3 major hurricane. While a favorable atmospheric environment (e.g., low vertical shear, elevated humidity) usually plays a leading role in TC intensification, we assess here the potential secondary impact that ocean conditions may have played in the intensification of Hurricane Maria over areas in the western North Atlantic Ocean using an experimental coupled ocean–hurricane model maintained by NOAA/AOML.

a. Model and observing system experiments

In this study, an experimental ocean–hurricane model is employed to assess the potential impact of ocean conditions on the intensity forecasts of Maria. The atmospheric component of the model, i.e., the Hurricane Weather Research and Forecasting

TABLE 2. Ocean OSEs developed with HYCOM used as initial conditions for the coupled HWRF-HYCOM simulations of Hurricane Maria carried out for the time period of 17–19 Sep 2017.

Expt	Description
No DA	HYCOM simulation initialized from a realistic ocean analysis (Navy global HYCOM) on 1 Jan 2017 and run through 31 Oct 2017 without ocean data assimilation
Add Alt	Initialized on 1 Jan 2017 by the No DA case and run through 31 Oct 2017 with assimilation of satellite altimetry observations following Cooper and Haines (1996)
Add Argo	Initialized on 1 Jan 2017 by the No DA case and run through 31 Oct 2017 with assimilation of Argo (Argo 2020) temperature and salinity profile observations
Add Gliders	Initialized on 1 Jan 2017 from the No DA case and run through 31 Oct 2017 with assimilation of temperature and salinity profiles from the NOAA/AOML underwater gliders starting on 12 Jul 2017 (see Fig. 2b)
All Obs	Initialized on 1 Jan 2017 by the No DA case and run through 31 Oct 2017 with assimilation of satellite altimetry and SST observations (U.S. Navy's MCSST), as well as temperature and salinity profile observations from underwater gliders and Argo floats

(HWRF) Model, is a specific configuration of the atmospheric community's Weather Research and Forecasting (WRF) Model dedicated to hurricane studies. HWRF has been used to study TC dynamics (e.g., Gopalakrishnan et al. 2011; Chen and Gopalakrishnan 2015; Halliwell et al. 2015; Smith et al. 2017) and to forecast TC path and intensity (e.g., Zou et al. 2013; Tallapragada et al. 2014). More recently, HWRF was coupled with the Hybrid Coordinate Ocean Model (HYCOM Bleck 2002; Halliwell 2004) to benefit from its data assimilation capability that enables a more realistic representation of the ocean state (e.g., Kim et al. 2014; Dong et al. 2017). HYCOM was implemented with the operational HWRF in 2012 for the western North Pacific region, and in 2017 for the Indian Ocean and Southern Hemisphere, to provide numerical guidance to forecasters with the Joint Typhoon Warning Center. For this study, we used HWRF version H218 coupled to an experimental HYCOM configuration maintained by NOAA/AOML. This HWRF version has three domains with increasing horizontal resolution (13.5, 4.5, and 1.5 km), with the inner two domains having higher resolutions that move with the storm. The NOAA/AOML HYCOM model domain covers the North Atlantic Ocean with 1/12° (~9 km) of horizontal resolution and 26 vertical levels and is configured following Halliwell et al. (2017a, 2020). For additional details about the coupled HWRF-HYCOM model and its configurations, please refer to the Supporting Material document.

We used outputs from various ocean model simulations with and without data assimilation (DA) as the initial ocean conditions for our HWRF-HYCOM coupled experiments. Such experiments are called Observing System Experiments (OSEs) and allow for assessing the impact of various observations on the representation of the ocean state (e.g., Halliwell et al. 2014). By initializing the coupled hurricane model with these different ocean states while using the same atmospheric conditions for all experiments, the impact of assimilating different ocean observations on subsequent hurricane experiments can be identified. The initial ocean conditions used within HWRF-HYCOM were extracted from various ocean OSE simulations performed in the North Atlantic hurricane region from 1 January to 31 October 2017, as summarized in Table 2. The coupled ocean–hurricane modeling experiments for Hurricane Maria were then carried out for the 17–20 September time frame, right before the storm made landfall in Puerto Rico on 20 September. We ran six cycles of hurricane simulations with the coupled HWRF-HYCOM model starting every 12 h between 0000 UTC 17 September and 1200 UTC 19 September 2017. Each cycle was initialized with five different ocean states from the various ocean OSE simulations (see Table 2) and provided a 5-day ocean–atmosphere coupled simulation of the storm. In total, 30 cycles of HWRF-HYCOM coupled experiments were carried out for Hurricane Maria. Using this methodology, we first assessed the impact of assimilating ocean observations on the representation of the ocean during Maria's passage (section 3b) and then on the potential impact of ocean conditions Hurricane Maria's intensity (section 3c).

b. *Representation of ocean conditions within the coupled model*

In this section, we analyze how the various ocean OSE simulations represent the ocean state. Following the state-of-the-art OSE approach, the impact of the assimilation of ocean observations from various platforms is estimated with respect to the unconstrained No DA simulation, in which no data are assimilated (e.g., Oke et al. 2009, 2015; Fujii et al. 2019). The free-running No DA simulation has been evaluated by Halliwell et al. (2017a) for being consistent with the observed ocean in a statistical sense (i.e., with comparable mean climatology and variability), so that it is a plausible realization of the ocean for the season, to which the data assimilative simulations can be compared.

Initial ocean conditions on 17 September 2017 for the No DA experiment east of the Lesser Antilles and Caribbean Sea were characterized by SSTs up to 1.5°C colder than satellite observations. Within our domain, the No DA experiment exhibited an SST error of $-0.6° \pm 0.7$°C (Fig. 7a), which is reported here as the mean bias ± the root-mean-squared error (RMSE). Moreover, the TCHP initialized by the No DA experiment exhibited a mean negative bias of -39.3 ± 20.9 kJ cm^{-2} (Fig. 7b), indicating the upper-ocean conditions simulated in this experiment were indeed much cooler than observations. Further comparison between the subsurface temperature structure from the No DA experiment with observations collected by the gliders confirmed that the temperature in the upper 200 m was 1°–4°C colder in the simulation than in the real ocean (Fig. 8a). By assimilating ocean observations, ocean

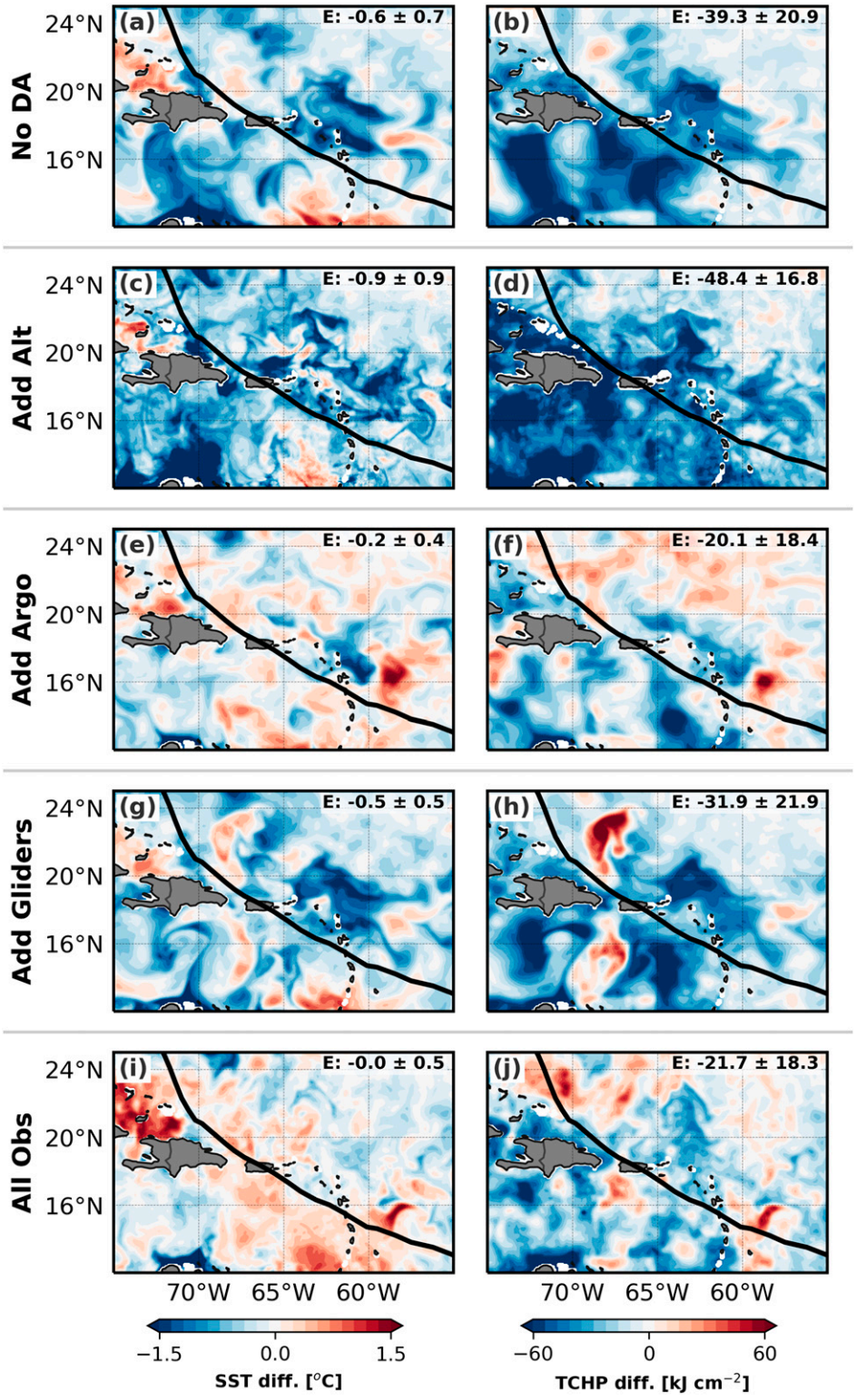

FIG. 7. HWRF-HYCOM ocean initial condition fields at 0000 UTC 17 Sep 2017, in terms of (left) sea surface temperature (SST) and (right) tropical cyclone heat potential (TCHP) differences with respect to satellite-derived observations for the (a),(b) No DA; (c),(d) Add Alt; (e),(f) Add Argo; (g),(h) Add Gliders; and (i),(j) All Obs experiments. Errors within the domain are shown in the upper-right corner for each variable as the mean bias plus and minus the root-mean-squared error.

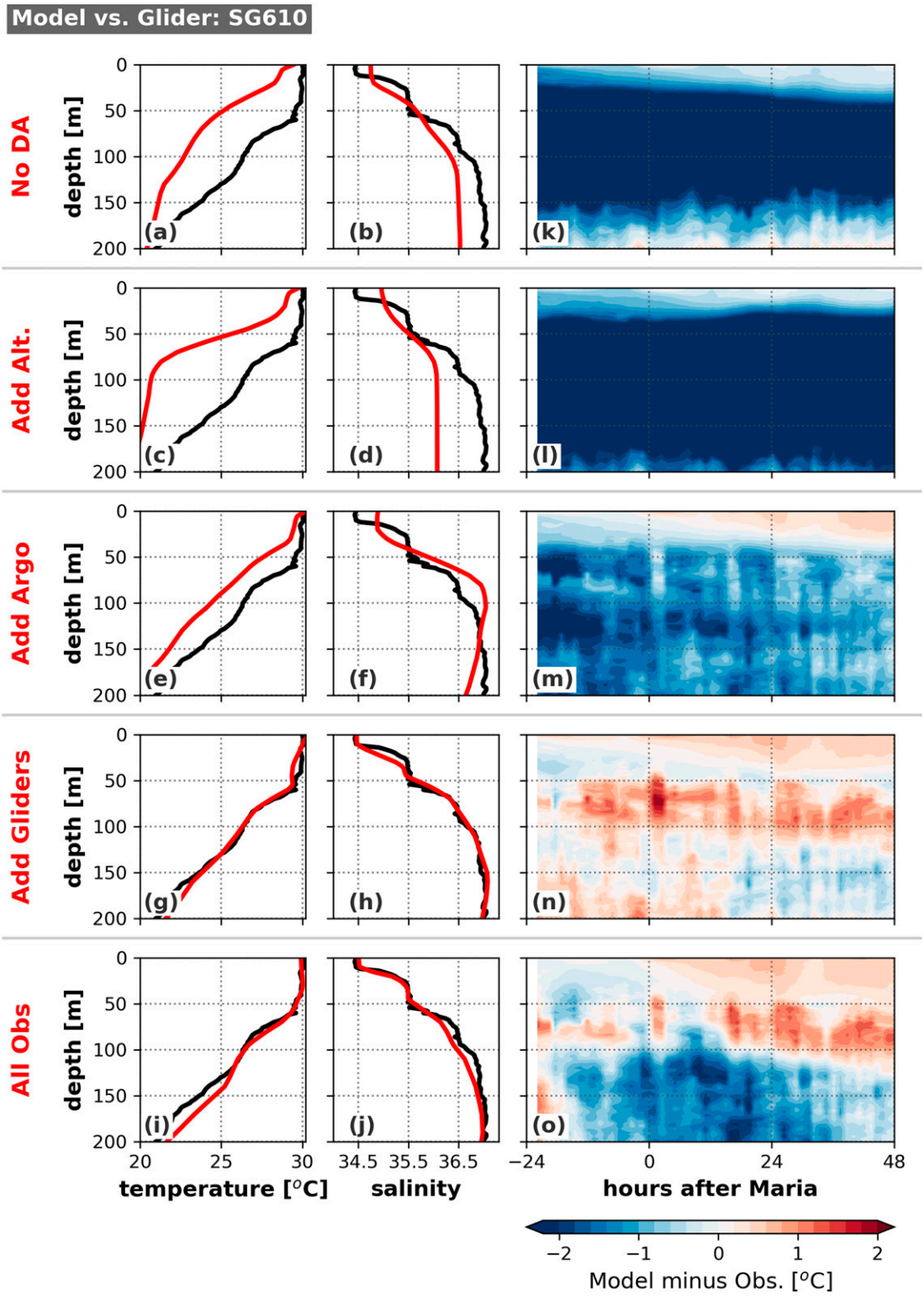

FIG. 8. (a)–(j) Temperature and salinity profiles 24 h before the closest approach from Hurricane Maria observed by glider SG610 (black lines, see Fig. 2b for location), compared with the initial conditions at the same location from the coupled HWRF-HYCOM model experiments developed in this study, initialized at 0000 UTC 17 Sep 2017 (red lines). (k)–(o) Difference in ocean temperature conditions before, during, and after the passage of Maria between the model for the various experiments and observations sampled by glider SG610.

TABLE 3. (top) Number of observation profiles from the three NOAA-operated gliders during the 24 h before and after the passage of Hurricane Maria. (bottom) Temperature root-mean-square error (RMSE) in the upper 100 m during the 24 h before and after the passage of Hurricane Maria from the coupled HWRF-HYCOM simulations starting at 0000 UTC 17 Sep 2017. RMSE estimates are based on observations collected along and in the vicinity of Maria's track by underwater gliders SG610, SG630, and SG635 (see Fig. 2b).

	Glider ID					
	SG610		SG630		SG635	
Time to TC	24 h before	24 h after	24 h before	24 h after	24 h before	24 h after
No. of profiles	18	20	20	21	22	23
Expt						
No DA	3.2°C	2.7°C	2.8°C	2.9°C	1.8°C	1.7°C
Add Alt	3.8°C	3.8°C	2.1°C	2.1°C	2.3°C	2.3°C
Add Argo	1.3°C	0.9°C	0.5°C	0.6°C	0.6°C	0.6°C
Add Gliders	0.5°C	0.6°C	0.7°C	1.1°C	0.4°C	0.4°C
All Obs	0.4°C	0.5°C	0.3°C	0.3°C	0.3°C	0.3°C

OSEs illustrate the impact of each component of the ocean observing system on the initial ocean fields used in the coupled forecasts of Maria. For instance, the assimilation of satellite altimetry observations in the Add Alt experiment generally led to corrections in the location of mesoscale ocean features (not shown). However, differences observed in the Add Alt experiment in terms of SST and TCHP with respect to satellite-derived observations exhibited similar values of $-0.9° \pm 0.9°C$ and of $-48.4 \pm 16.8\ kJ\ cm^{-2}$ (Figs. 7c,d) as in the No DA experiment (Figs. 7a,b). This indicates that the assimilation of altimetry observations alone cannot correct the upper-ocean thermohaline structure. In the vertical, the comparison of upper-ocean conditions (top 200 m) from the Add Alt experiment with glider observations showed that the simulated temperature was still 1°–4°C colder in the model than in the real ocean (Fig. 8c). Interestingly, cold biases simulated in Add Alt were larger than the ones simulated in experiment No DA. Therefore, one of the main results reported here based on comparisons with both satellite observations (Fig. 7) and in situ subsurface profiles from gliders (Fig. 8) is that the specific initialization of the coupled-model with no ocean data assimilation in our HYCOM model configuration leads to overall cold temperature biases in the upper ocean and that such biases are not corrected by the assimilation of altimetry observations alone. Results from subsequent Add Argo and Add Gliders experiments produced a consistent error reduction in terms of SSTs and TCHP (Figs. 7e–h, Table 3) when compared to the No DA and Add Alt experiments (Figs. 7a–d). The assimilation of Argo or glider observations led to a 0.5°–1.5°C (Fig. S5e,g) and 20–50 $kJ\ cm^{-2}$ (Fig. S5f,h) warming of upper-ocean conditions when compared to the No DA case; however, these corrections were mostly observed in areas directly in the vicinity and downstream from the glider's location in the Add Gliders experiment. Temperature errors in the ocean initial conditions were generally observed to persist in the coupled experiments of Hurricane Maria within the HWRF-HYCOM model (e.g., Figs. 8k–o).

We conducted an additional quantitative assessment on the accuracy of the ocean representation within the unconstrained (No DA) and data aggregation OSEs (Add Alt, Add Argo, Add Gliders, All Obs) based on comparisons with more than 120 profiles collected by three underwater gliders in the vicinity of Maria's track (Fig. 2b). The comparison focused on the representation of temperature conditions 24 h before and after Maria in the top 100 m, which is the water layer where strong hurricane-induced mixing is usually observed (e.g., Fig. 3 in Domingues et al. 2015). Results from this analysis are summarized in Table 3. They revealed that ocean temperature conditions observed in the upper 100 m using the No DA experiment showed a RMSE of 3.2°C at the location of glider SG610 (Fig. 8k) and of 2.8°C for glider SG630 (Fig. S6k), both in the Caribbean Sea during the 24 h preceding Maria. In the tropical North Atlantic Ocean at the location of glider SG635, the RMSE was slightly smaller with a value of 1.8°C (e.g., Fig. S7k). For the Add Alt experiment, the assimilation of altimetry observations failed to correct temperature biases in the top 100 m: RMSE values of 2.1°–3.8°C were observed in the Caribbean Sea, while a value of 2.3°C was observed in the tropical North Atlantic Ocean (Table 3).

The assimilation of profile observations from Argo floats led to major improvements in the subsurface representation of temperature conditions (e.g., Fig. 8m). With Argo profiles assimilated into the Add Argo experiment, the RMSE in the upper 100 m was reduced to 0.5° and 1.3°C in the Caribbean Sea at the location of gliders SG630 and SG610, respectively, and 0.6°C in the tropical North Atlantic Ocean at the location of glider SG635. These error reductions amounted to more than a 50% improvement with respect to temperature conditions for the No DA and Add Alt cases (Table 3). The Add Gliders experiment exhibited RMSE values of 0.5°–0.7°C for the Caribbean Sea and 0.4°C for the tropical North Atlantic Ocean, while the All Obs experiment exhibited values of 0.3°–0.4°C for the Caribbean Sea and 0.3°C for the tropical North Atlantic (Table 3, Figs. 8g–j,n,o). We note that, following the coupled model initialization, temperature errors are observed to slightly increase as a function of simulation time. This is an expected outcome, given that results from the coupled simulations are strictly propagated forward in time by model physics, and are not constrained by ocean data assimilation. Hence, simulated ocean conditions at this stage are expected to diverge from observations with time. Despite the increasing errors, the smaller errors during model initialization verify that the assimilation of ocean data produces the expected corrections at the location

of the gliders. Upper-ocean temperature corrections resulting from glider data assimilation were observed to impact the ocean not only at the location of the gliders, but also in the vicinity and downstream of where these observations were collected in the Caribbean Sea and tropical North Atlantic Ocean (see Fig. S5).

c. *Coupled ocean–hurricane experiments for Hurricane Maria*

In this section we analyzed the proof-of-concept coupled ocean–hurricane experiments of Hurricane Maria in terms of hurricane characteristics. For informational purposes, we include with our results the real-time NHC forecasts issued for Maria in September 2017. We note, however, that the official NHC forecasts take into account results from several operational model ensembles, real-time satellite and airplane survey observations, and the personal judgment from forecasters. Therefore, the NHC forecasts are inherently distinct and not directly comparable to our results.

1) Results from the 0000 UTC 17 September 2017 cycle

We assess first results from a specific simulation cycle starting at 0000 UTC 17 September 2017, which enables carrying out a more detailed analysis and yields an initial understanding of potential impacts of the observed ocean conditions in the simulation of Hurricane Maria. Considering the hurricane track (Fig. 9a), results showed that assimilation of ocean observations led only to small changes in the simulated track. In fact, both All Obs and No DA experiments simulated a track displaced northward from the observed best track. Ocean conditions were expected to have a limited impact on the hurricane track, given that Maria was mostly steered by large-scale atmospheric flow like most hurricanes (e.g., Kasahara and Platzman 1963; Shapiro 1982). Large-scale atmospheric flows are included in our experiments as initial and boundary conditions provided by forecast cycles from the NOAA's Global Forecast System (GFS) model. One practical implication from the displacements in track in the All Obs and No DA simulations is that the eye of Maria, for this specific simulation cycle, passed to the east of Puerto Rico and over the Virgin Islands (Fig. 9a).

While the assimilation of ocean observations led to small changes in the simulated track of Maria, the impact on simulated storm intensity was more pronounced (e.g., Fig. 9b). For the same simulation cycle initialized at 0000 UTC 17 September 2017, both the All Obs and No DA experiments showed a period of intensification at the beginning of their respective simulation until 19 September. However, in the All Obs experiment, which was initialized following the assimilation of all available ocean observations, Maria reached category-4 intensity on 19 September (red line, Fig. 9b). For the same time period, the No DA experiment projected Maria with category-3 intensity (blue line, respectively, Fig. 9b). Compared to Maria's observed maximum winds of 145 kt on 19 September, the All Obs experiment projected a maximum wind speed of 117 kt, while the No DA experiment projected 105 kt. The overall better performance of the All Obs experiment for the cycle initialized

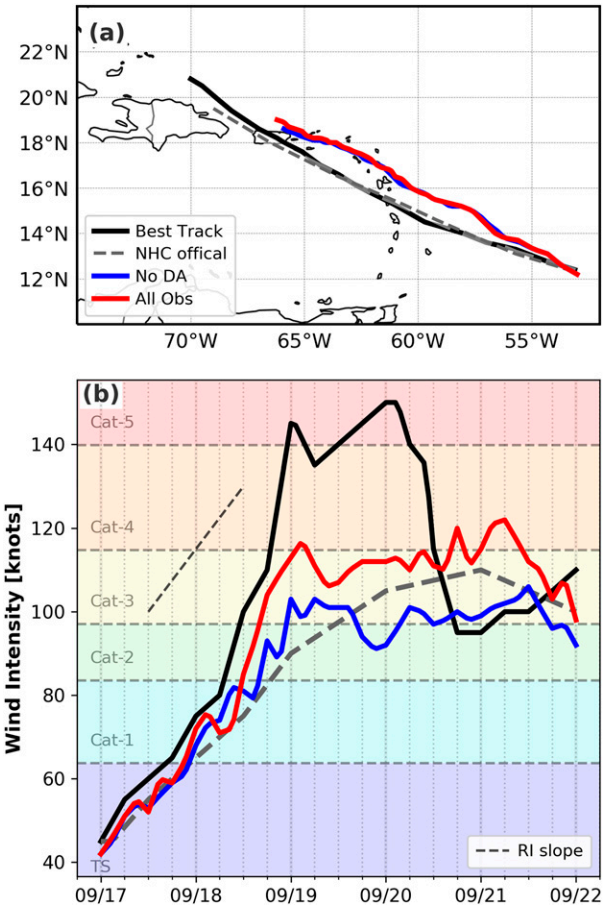

FIG. 9. Coupled model results for Hurricane Maria (2017). Example of a simulation cycle starting at 0000 UTC 17 Sep. (a) Track of the storm as observed (solid black line) and as simulated from two experiments: No DA (blue line) and All Obs (red line) (see text for details about the experiments). (b) Intensity (maximum wind speed, kt) of the storm as observed and as simulated by the same experiments. The forecasted location and intensity from the National Hurricane Center (NHC) at the time of the storm are marked with a dashed gray line, for reference. The black dashed line in the upper-left corner of (b) indicates the slope of TC rapid intensification (30 kt in 24 h).

at 0000 UTC 17 September 2017 was partly associated with the more accurate representation of the rate of TC intensification, which was more comparable to observations during the 17–19 September period. The No DA experiment only showed comparable TC intensification rates during the first day of the simulation (Fig. 9b).

2) Impact of ocean conditions on air–sea enthalpy fluxes

To assess in detail the physical processes that contributed to the higher projected intensity of Maria in the All Obs experiment compared to the No DA experiment, we analyzed the total ocean–hurricane enthalpy flux over the 24–30 h period for the same simulation cycle starting at 0000 UTC 17 September 2017 (Figs. 10a,b). We focused on this time window because it corresponded to the timing for when the intensity projected by

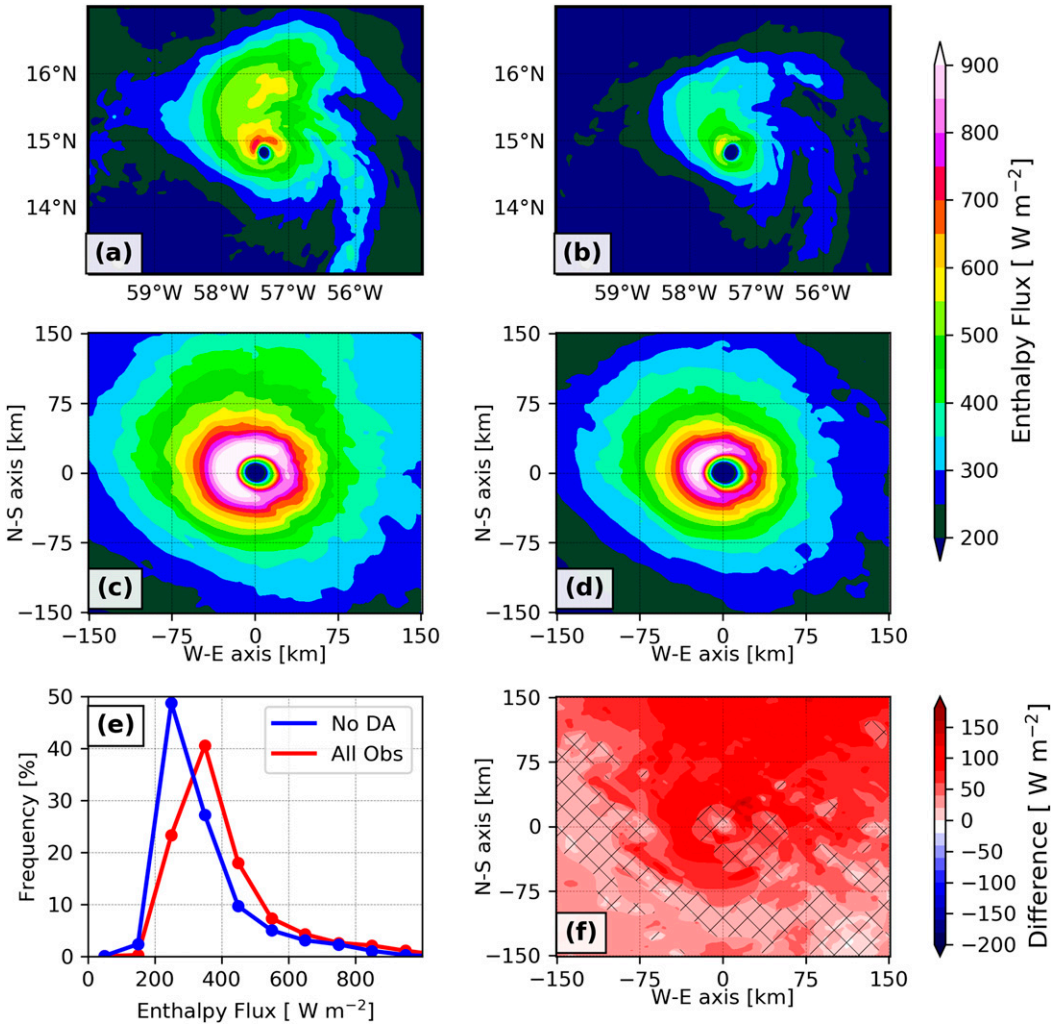

FIG. 10. Total ocean–hurricane surface enthalpy flux for Hurricane Maria (2017) derived from coupled experiments developed in this study. (a),(b) The total enthalpy flux averaged over the 24–30 h period for the simulation cycle starting at 0000 UTC 17 Sep 2017 for the All Obs and No DA experiments, respectively. (c),(d) The composite enthalpy flux for experiments All Obs and No DA, respectively, in a storm-centric coordinate system for all six simulation cycles computed during the 6 h period right before intensity bifurcation in each cycle. (e) Distribution of enthalpy flux within 150 km from the center considering all six simulation cycles sampled during the 6 h period right before intensity bifurcation in each cycle for experiments All Obs (red line) and No DA (blue line) binned every 100 W m^{-2}. (f) Mean difference in enthalpy fluxes between All Obs and No DA calculated as the difference for individual cycles, and then averaged. Hatched areas in (f) highlight areas where the enthalpy flux differences are not statistically significant at the 95% confidence level, considering all simulation cycles.

the All Obs simulation diverged from the one by the No DA simulation. The analysis revealed that surface enthalpy fluxes were substantially larger in the All Obs simulation (Fig. 10a) when compared to the No DA simulation (Fig. 10b). Enthalpy fluxes near the eyewall were ~700–800 W m^{-2} in the All Obs simulation and ~500–600 W m^{-2} in the No DA simulation. Fluxes in the hurricane outer bands were ~500–600 W m^{-2} for the All Obs simulation and of ~300–400 W m^{-2} for the No DA simulation. This indicates that the improved representation of SSTs and upper-ocean conditions in the All Obs experiment (e.g., Figs. 7i,j and 8), which was achieved through ocean data assimilation, ultimately led to an enhanced portrayal of Maria's surface enthalpy fluxes for the simulation cycle starting at 0000 UTC 17 September 2017. The stronger enthalpy flux favored an intensified and healthier deep convection, contributing to the development of a stronger TC. This explains why the intensity achieved by Maria in the simulation cycle starting at 0000 UTC 17 September 2017 was higher in the All Obs simulation when compared to the No DA simulation (Fig. 9b).

To further investigate to what extent ocean data assimilation led to higher enthalpy fluxes during September 17–19, we extend the analysis above by: 1) calculating enthalpy flux composites using all 6 simulation cycles from both All Obs and No DA experiments in a storm-centric coordinate frame, and using a

6 h averaged window before the intensity bifurcation (defined as wind speed difference > 20%) in each cycle (Figs. 10c,d), 2) analyzing the distributions of combined enthalpy fluxes from the 6 simulation cycles for the same 6 h window (Fig. 10e), and 3) estimated the mean difference in enthalpy fluxes between All Obs and No DA, calculated as the difference for individual cycles averaged over all cycles (Fig. 10f). Results from the composite analysis confirms that, considering all simulation cycles, enthalpy fluxes are consistently 25–100 W m^{-2} (10%–20%) larger in the All Obs simulation (Fig. 10c) when compared to the No DA experiment (Fig. 10d). In fact, further analysis shows that the enthalpy flux distribution from experiment All Obs is partially shifted toward larger values in relation to the distribution from the No DA experiment. For instance, in experiment No DA, the distribution has a mean of 341.6 W m^{-2} and peaks at approximately 250 W m^{-2} (blue line, Fig. 10e), while in experiment All Obs the distribution has a mean of 400.5 W m^{-2} and peaks at ~350 W m^{-2} (red line, Fig. 10e). These two distributions are statistically distinct ($p < 0.01$) based on a doubled-tailed t test, and a Kolmogorov–Smirnov test (Hodges 1958). In addition, the mean enthalpy flux differences, calculated as the difference from individual cycles, reveals that the enthalpy fluxes are in fact at least 50 W m^{-2} larger in most parts of the simulated storm, and up to 150 W m^{-2} larger in some locations. Further statistical analysis reveals that such differences are statistically significant at the 95% significance level in most parts of the simulated hurricane, and especially at the eyewall and upper-right quadrant, which is generally the most intense quadrant for Northern Hemisphere TCs.

3) Experiments skill assessment

A more robust and quantitative skill assessment was carried out for each coupled experiment (e.g., Table 2) based on six simulation cycles between 17 and 19 September (Fig. 11). For each type OSE coupled hurricane–ocean simulation, we estimated the RMSE as the square root of the mean square differences between the simulated hurricane wind intensity in each cycle and the best track observations (black line, Fig. 9). To gain additional insight in the No DA and All Obs experiments, the total RMSE is also decomposed, following Halliwell et al. (2017a), into a mean bias and residual errors that can be associated with the coupled model uncertainty. RMSE calculations were referenced as a function of lead forecast time (Fig. 11a), as routinely reported for operational forecasts (see https://www.nhc.noaa.gov/verification/verify5.shtml), and also as a function of date (Fig. 11b), which allow us to identify potential improvements in the simulation of Maria's intensity before it made landfall in Puerto Rico at ~1200 UTC 20 September 2017. It is worth acknowledging that the RMSE presented in terms of date combines results from simulations with different lead times, which inherently present different levels of degradation from original initial conditions (e.g., Fig. 11a). However, this analysis allows us to more closely assess the value of underwater glider observations for improvements during the 24 h prior to landfall, given that these vehicles surveyed areas closer to Puerto Rico, potentially impacting that specific part of Hurricane Maria's track.

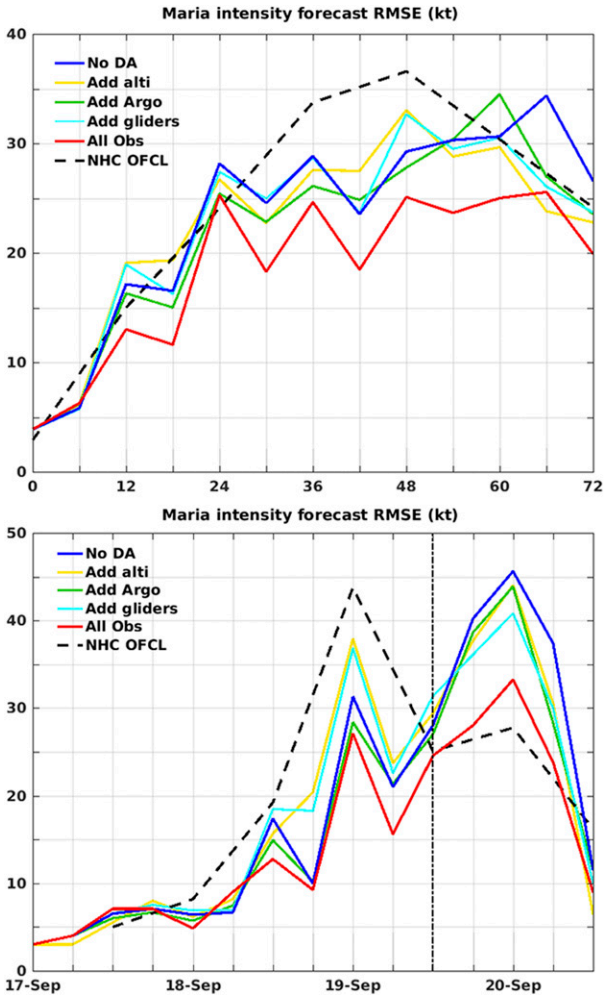

FIG. 11. Coupled model results for Hurricane Maria (2017): root-mean-square error (RMSE) in intensity (maximum wind speed, kt) with respect to observations. (top) RMSE, in terms of simulation lead time, for the first 72 h. (bottom) RMSE represented as a function of simulation date during 17–20 Sep. The RMSE from the various experiments are as follows: No DA (dark blue line), Add Alt (yellow line), Add Argo (green line), Add Gliders (cyan line), and All Obs (red line) (see text for details about the experiments). The vertical dot–dashed black line marks the approximate 24 h prior to Maria's landfall in Puerto Rico, between 1200 UTC 19 Sep and 1200 UTC 20 Sep 2017. The RMSE for all NHC forecasts (from 0 to 120 h lead times) valid at each given time and date is shown as a dashed black line, for reference.

The RMSE with lead times between 0 and 72 h for simulations developed in this study for Hurricane Maria was, on average, 23.0 kt for the No DA case, (dark blue line, Fig. 11a), which is decomposed into a −11.6 kt mean bias, and 19.0 kt in residual errors. The RMSE for experiment No DA was the highest value among all the experiments. On the other hand, the lowest RMSE of 18.5 kt was obtained when all available ocean observations were assimilated into the All Obs experiment (red line, Fig. 11a), with the mean bias reduced to −6.0, and 16.5 kt in residual errors. In other words, the more accurate

representation of ocean conditions, achieved through assimilation of all ocean observations, led to an improvement in the 72 h representation of Maria's intensity. Most of the improvement is attributable to corrections of the negative intensity biases, which are smaller in the All Obs experiment, whereas the residual errors that associate with model uncertainty are of similar magnitude in both experiments (19 kt in No DA and 16.5 kt in All Obs). These results are consistent with what was expected from the ocean data assimilation, which helped correct the upper-ocean cold temperature biases observed in No DA (e.g., Figs. 7 and 8) and ultimately lead to larger enthalpy fluxes (Fig. 10).

The intensity errors estimated from the different experiments based on the assimilation of data from individual ocean observing platforms, showed varying performances throughout the 72 h simulation period (Fig. 11a). On average, the assimilation of altimetry data in the Add Alt experiment was associated with an RMSE of 22.4 kt (yellow line, Fig. 11a). Argo profile data assimilated in the Add Argo experiment resulted in an RMSE of 21.8 kt (green line, Fig. 11a), while glider data assimilated in the Add Glider experiment produced an RMSE of 22.5 kt (cyan line, Fig. 11a). An additional experiment developed with the assimilation of satellite-derived SST data alone resulted in an RMSE of 21.7 kt for the 72 h window (not shown).

The RMSE in terms of simulation date showed that error levels from the various experiments peaked within the 24 h preceding landfall (Fig. 11b), while different performances were observed for other time windows of our experiments. During the 24 h preceding landfall, the unconstrained No DA simulation had the largest RMSE of 33.7 kt, while assimilation of all available ocean observations in the All Obs experiment led to the lowest RMSE of 23.5 kt. The various OSEs allowed for us to estimate the specific contribution from each observing platform toward improving the simulated intensity of Maria. Specifically: 1) the assimilation of altimetry data in the Add Alt experiment had an RMSE of 29.7 kt, contributing ~33% of the total error reduction achieved by the All Obs experiment; 2) assimilation of Argo profiling data in the Add Argo experiment led to an RMSE of 30.6 kt, contributing ~27% of the total error reduction achieved by the All Obs simulation; and 3) assimilation of glider data in the Add Gliders simulation led to an RMSE of 29.2 kt over the same period, contributing ~40% to the total error reduction achieved by the All Obs simulation. Assimilation of satellite-derived SST data alone also resulted in an RMSE of 30.6 kt for the 24 h window (not shown), similar to the Add Argo experiment. Thus, in the 24 h preceding the landfall of Hurricane Maria, ocean gliders deployed near Puerto Rico were the main contributor to the error reduction achieved by the assimilation of ocean observations. Results shown here are for glider profile observations that are in the vicinity (1°–2°) of the hurricane track and, therefore, have a larger impact for that specific timeframe (Halliwell et al. 2020). Similarly, Argo observations enabled the largest error reduction at their time and locations in areas ahead of Hurricane Maria, except during the 24 h preceding landfall (Fig. 11b). This highlights the importance of analyzing and assimilating data from observing platforms that provide profile data with different spatial and temporal sampling strategies.

4. Discussion

Hurricanes Irma, Jose and Maria were among some of the major Atlantic hurricanes from 2017 that intensified in a favorable atmospheric environment characterized by relatively low vertical wind shear and elevated relative humidity in the lower atmosphere (Landsea 2017; Berg 2017, 2018; Cangialosi et al. 2018; Pasch et al. 2019). Associated with the favorable atmospheric environment, warm SST anomalies that existed in the North Atlantic were shown to be a key factor determining the major hurricane activity observed in 2017 (Murakami et al. 2018). In addition, we have shown that Irma, Jose, and Maria reached their respective maximum intensity while traveling over areas that were also characterized by high TCHP values above 50 kJ cm^{-2} and SSS below 35, which are known for helping maintain SSTs warm and sustain TC intensification when the atmospheric environment is also favorable. While warm SSTs and high TCHP indicate the amount of energy potentially available to fuel TC intensification (e.g., Shay et al. 2000; Mainelli et al. 2008), low SSS is indicative of the existence of barrier layers that can help maintain warm SSTs and sustain enthalpy fluxes from the ocean into the hurricane (e.g., Ffield 2007; Balaguru et al. 2012; Reul et al. 2014a; Domingues et al. 2015). These three overlapping ocean conditions (e.g., Figs. 1 and 2), when combined with a low-shear and favorable atmospheric environment for Irma (Landsea 2017; Cangialosi et al. 2018), Jose (Berg 2018), and Maria (Berg 2017; Pasch et al. 2019), provided sufficiently favorable conditions that likely contributed to their rapid intensification over areas west of 55°W within the tropical North Atlantic Ocean and Caribbean Sea. Underwater glider observations sampled in the outskirts of these three hurricanes and satellite-derived observations indicate that these prestorm conditions partly suppressed the hurricane-forced SST cooling, which was generally below 1°C (e.g., Figs. 5b, 6). Therefore, Hurricanes Irma, Jose, and Maria consistently experienced SSTs larger than 28°C throughout these areas. Other hurricanes that intensified while traveling over areas with similar ocean conditions include Omar (2008) (Balaguru et al. 2012), Gonzalo (2014) (Domingues et al. 2015), Michael (2018) (Goni and Domingues 2019), and several additional hurricanes that passed through the Caribbean Sea (Ffield 2007; Rudzin et al. 2019).

Our analysis indicates that the areas where Hurricanes Irma, Jose, and Maria reached their peak intensity showed more favorable ocean conditions than normal for hurricane intensification when compared to the historical record (e.g., Fig. 3). These areas of the tropical North Atlantic Ocean have been consistently warming over the past several decades (e.g., Good et al. 2007; Polyakov et al. 2010). In fact, the subtropical North Atlantic Ocean and Atlantic warm pool experienced a substantial warming during 2010–15 that was caused by heat convergence associated with changes in the meridional heat transport (Domingues et al. 2018; Volkov et al. 2019). This upper-ocean warming continued after 2015 (not shown). In addition, recent intensifications in the riverine discharge from

the Amazon (Gouveia et al. 2019) and Orinoco (Gallay et al. 2019) have been recorded over the past few years which, for the Amazon plume, has contributed to an overall salinity freshening of 3.5% yr^{-1} in the main plume water export pathway. Intense mesoscale activity from North Brazil Current rings (e.g., Fig. S2) normally observed in the region (e.g., Goni and Johns 2001) have further promoted the increase in the extension of the low salinity plume, as observed in 2017 (Fig. 1c). The combination of warm SSTs and large riverine discharge from the Amazon–Orinoco has been previously recognized as potential factors controlling interannual fluctuations in major hurricane activity in the North Atlantic (e.g., Ffield 2007; Reul et al. 2014a), and 2017 served as an excellent example confirming the increased hurricane activity when such conditions are available. However, it is important to emphasize that these specific ocean conditions complemented the availability of a favorable atmospheric environment experienced by Irma (Landsea 2017; Cangialosi et al. 2018), Jose (Berg 2018), and Maria (Berg 2017; Pasch et al. 2019), which likely played a dominant effect in enabling their intensification.

The proof-of-concept coupled model experiments developed in our study for Hurricane Maria yielded results that are consistent with previous knowledge that the ocean can play a crucial role in modulating hurricane intensification (e.g., Mainelli et al. 2008; Dong et al. 2017). Specifically, our results showed that by varying the ocean representation among different numerical experiments, while using the same favorable atmospheric conditions observed for Hurricane Maria (Berg 2017; Pasch et al. 2019), the hurricane intensity was more/less accurately reproduced. This is partly explained because ocean model initialization errors generally lead to large errors in predicted SSTs under TCs (Halliwell et al. 2008, 2011), which, as our results showed, can translate into changes in enthalpy fluxes under a TC (Fig. 10). In addition, previous studies using idealized coupled simulations demonstrated that barrier layers can, in fact, favor further intensification by up to 15% in category-1 hurricane strength or greater because of the reduced SST cooling below the TC inner core (Hlywiak and Nolan 2019). Upper-ocean stratification was also found to be a key factor determining the air–sea coupled feedback on coupled-simulations of the western Pacific typhoons Haiyan (2013) and Neoguri (2014) (Mogensen et al. 2017), and for the Atlantic Hurricane Gonzalo (2014, Dong et al. 2017). These results for Hurricane Maria provide an additional case study demonstrating that representing both the upper-ocean thermal and salinity stratification accurately within coupled models is relevant for obtaining improved simulations of hurricane intensity.

The ocean OSEs carried out in our study also allowed us to quantify, for a single hurricane, the potential impact that different components of the global ocean observing system can have on reducing ocean model initialization errors and the subsequent impacts on coupled ocean–hurricane simulations. While a comprehensive analysis of multiple TCs is still required to confirm any robust improvements in the hurricane intensity simulations, our results for Hurricane Maria, and initialized with different ocean OSEs, demonstrated that intensity errors for this specific hurricane were reduced during the 3-day simulation when all ocean observations were assimilated. Our results demonstrated that by assimilating individual components of the observing system, each tended to slightly reduce intensity errors, and optimal results were obtained when all components of the ocean observing system were assimilated. Previous analysis by Halliwell et al. (2017a) indicated that the assimilation of satellite altimetry data provides the largest contribution for correcting mesoscale structures in the model, and that the correction of upper-ocean temperature and salinity biases required assimilation of profile observations sampled in sustained mode, such as those from Argo floats or gliders. Further analysis in Halliwell et al. (2020) also showed that a single ocean platform can produce corrections within a limited spatial extent of 1°–2° around the instrument. In other words, the area where a forecasted hurricane will experience the benefit from the assimilation of glider observations is limited to the vicinity of where the observations are collected. Assimilation of both Argo and glider observations in sustained mode in our study enabled substantial reductions in subsurface temperature biases (Table 3, Fig. 8), supporting larger air–sea enthalpy fluxes (Fig. 10), and improved intensity simulation of Hurricane Maria. Our results, therefore, further highlight the importance of sustained ocean observations in support of TC studies and forecasts (see Domingues et al. 2019). Targeted underwater glider networks help fill this need by providing particularly valuable observations in the vicinity of populated areas which may be affected by a landfalling hurricane. In fact, our results for the 24 h time period that preceded Maria's landfall showed that assimilation of glider data alone led to an average error reduction of 4.5 kt in wind speed, which represented the maximum contribution from an individual observing platform toward improving the simulated intensity of Maria (Fig. 11b). This is partly due to the limited number of profile observations available from other observing platforms for the time of this particular analysis. However, the density of glider observations enables more frequent assimilation in the model, which is not matched by any other component of the ocean observing system.

Finally, our study also adds to other recent efforts by the community that focus on improving simulations of hurricane intensification, such as through enhancements of model physics parameterizations within atmospheric models and a reduction in initialization errors using atmospheric data assimilation (e.g., Gopalakrishnan et al. 2011; Zhang et al. 2015; Christophersen et al. 2018; Cucurull and Mueller 2020). For example, previous studies have shown that (i) assimilation of surface wind data from NASA's Cyclone Global Navigation Satellite System improved the simulated track and intensity of Hurricanes Harvey and Irma (2017) by as much as ~20% (Cui et al. 2019); and (ii) assimilation of Global Hawk dropwindsondes enabled a better representation of the location, intensity, and wind–pressure relationships within the hurricane, with an overall skill improvement ranging from 25% to 35% (Christophersen et al. 2018). Ultimately, both ocean and atmospheric OSEs enable the identification of key components of the observing system needed to support hurricane studies.

5. Conclusions

Satellite and in situ ocean observations were analyzed to first assess the ocean conditions in the tropical Atlantic and

Caribbean Sea before, during, and after the passage of the 2017 major Atlantic Hurricanes Irma, Jose, and Maria. Our analysis then proceeded to evaluate the impact of these observations in the representation of the upper-ocean conditions within the HYCOM ocean model based on different sets of observing system experiments (OSEs), where either all or individual components of the ocean observing system were assimilated. Ocean OSEs then provided the initial ocean conditions for proof-of-concept coupled experiments of Hurricane Maria using HWRF-HYCOM, which allowed us to evaluate the impact of the ocean, including the contribution from individual ocean observing platforms, in the coupled ocean–hurricane simulation of Maria's intensity. The key findings of our study are the following:

- Hurricanes Irma, Jose, and Maria reached their peak intensity in a relatively favorable atmospheric environment and also while traveling over ocean areas with more favorable conditions than normal for TC intensification.
- Widespread low-salinity conditions were present during the passage of these hurricanes off the Virgin Islands, Puerto Rico, and the Dominican Republic, and were associated with an above normal extension of the Amazon and Orinoco riverine plumes, that form surface barrier layers that can contribute to TC intensification.
- In addition to the barrier layer, the region of study was characterized by large SST and TCHP values, of 28°C or higher and above 60 kJ cm^{-2}, respectively.
- The optimal representation of such ocean conditions presented during the period of study within the HYCOM ocean model was achieved through the assimilation of in situ ocean observations, particularly ocean profiles of temperature and salinity, and satellite measurements of SST and SSH. Without ocean data assimilation, the ocean component of coupled experiments was generally too cold in the experiments carried out in this work, with negative biases of $-0.6° \pm 0.7$°C for SST and -39.3 ± 20.9 for TCHP. Assimilation of satellite altimetry observations alone allowed for an improved representation of the location of mesoscale ocean features. However, in our specific modeling system, the assimilation of altimetry observations was unable to correct large-scale cold biases or to identify barrier layers.
- Assimilation of in situ ocean profiles corrected subsurface temperature and salinity biases. Corrections to large-scale biases were accomplished through assimilation of Argo profiles, and improvements near the glider locations (including up to 50% additional error reduction) were achieved by assimilating the glider observations.
- The optimal upper-ocean representation was achieved when all observations from gliders, altimetry, and Argo, were jointly assimilated into the model.
- The improved ocean representation achieved with the assimilation of ocean observations ultimately led to an improvement in the 72 h simulation of Maria's intensity, with more notable improvement during the 24 h time-window that preceded Maria's landfall in Puerto Rico.
- The correct representation of upper-ocean conditions enabled simulating more realistic ocean–atmosphere enthalpy fluxes for Hurricane Maria, ultimately leading to a reduction in intensity errors during the 24 h preceding landfall in Puerto Rico.
- The assimilation of underwater glider observations alone provided the single-most individual contribution toward the total error reduction during the 24 h time frame before landfall achieved by assimilating all observations. These results were obtained by assimilating data from two gliders deployed in the Caribbean Sea south of Puerto Rico, and one to the north of where Maria traveled (Fig. 2b).

These OSE-based results provide quantitative evidence that different components of the ocean observing system can jointly provide valuable information about upper-ocean conditions in support of improved TC simulations. For example, satellite altimetry helps constrain conditions in terms of mesoscale ocean features, Argo data provide valuable information to correct large-scale temperature and salinity biases in the model, and glider data enable corrections for high-resolution temperature and salinity biases, their horizontal gradient, and location of barrier layers in regions where hurricanes travel and intensify. To the best of our knowledge, very few ocean OSEs have been conducted to date to document the impact of improved ocean representation in coupled ocean–hurricane forecast models. Therefore, this research helps to address a critical need, and provides a valuable resource for the ocean and hurricane research and forecasting community.

The results presented herein were based on six simulation cycles, complementing results by Dong et al. (2017). The consistent impact of assimilating ocean observations revealed by these cases provides an additional argument for conducting similar ocean–hurricane coupled experiments for a much larger number of realizations (multiple simulation cycles over multiple storms, in addition to Jose and Irma) to provide robust, statistically significant assessments of observing system impacts and demonstrate potential robust improvements to future forecast systems.

Finally, observing system simulation experiments (OSSEs) (e.g., Halliwell et al. 2014; Cucurull and Mueller 2020) provide a critical tool for designing optimal sampling strategies in support of TC studies, with initial results recommending the collection of temperature and salinity profiles from moving platforms every 1° to maximize the effect of ocean profile data assimilation into ocean models (e.g., Halliwell et al. 2017b). For example, had Maria occurred in 2019 when more than 10 gliders operated by NOAA/AOML, the U.S. Navy, the U.S. Integrated Ocean Observing System (IOOS), Rutgers University, and the University of Miami surveyed areas under Maria's track (see https://gliders.ioos.us/map/), it could be hypothesized that the overall impact of glider observations on Maria's simulations would likely have been even larger.

Hence, underwater gliders provide a key tool for maintaining such spatial coverage since, unlike Argo floats that drift with the currents, they can be positioned to maintain sufficient spatial resolution along predetermined tracks. Therefore, results obtained in this type of study illustrate the potential benefit of sustaining an ocean observing system in the North Atlantic Ocean and Caribbean Sea dedicated to hurricane research.

Such a system has the potential to significantly reduce errors in how the ocean is represented within coupled models over much larger areas, helping to better monitor and simulate storm characteristics for longer periods during the life cycle of Atlantic hurricanes.

Acknowledgments. This work was supported by the NOAA Atlantic Oceanographic and Meteorological Laboratory (Miami, FL), the NOAA Office of Atmospheric and Oceanic Research (OAR), and the NOAA Quantitative Observing System Assessment Program (QOSAP). It was also supported by the Disaster Related Appropriation Supplemental: Improving Forecasting and Assimilation (DRAS 19 IFAA), awarded to NOAA-AOML, to the University of Miami under Awards NA19OAR02201840 and NA19OAR0220186. It was also supported by the FY19 Disaster Supplemental: Improving Forecasting of Hurricanes, Floods, and Wildfires (FY 19 IFHFW) awarded to NOAA-AOML and to the University of Miami under Award NA20OAR4600263. R. Domingues, M. Le Hénaff, and J. Zhang were partly supported under the auspices of the Cooperative Institute for Marine and Atmospheric Studies (CIMAS), a cooperative institute of the University of Miami and NOAA, Cooperative Agreement NA20OAR4320472. J. Zhang was also partly supported by NSF Grant AGS1822128 and ONR Grant N00014-20-1-2071. The authors thank the NOAA and CIMAS personnel who contributed in various ways to the success of underwater glider operations and to the acquisition and processing of their data: Ulises Rivero, Grant Rawson, Diego Ugaz, Patrick Halsall, and Caridad Ibis Gonzales. The authors are also grateful to all of the individuals who participated in the deployment and recovery of the underwater gliders. Finally, the authors thank three anonymous reviewers for their thorough reviews that greatly helped enhance this manuscript.

Data availability statement. SST data used in the observational analysis are from NOAA's High-Resolution Optimally Interpolated SST, version 2 (available at: http://www.esrl.noaa.gov/psd/). The SST assimilated in HYCOM is the AVHRR multichannel sea surface temperature (MCSST) product made available by the U.S. Navy Fleet Numerical Meteorology and Oceanography Center (FNMOC, available at https://nrlgodae1.nrlmry.navy.mil/cgi-bin/datalist.pl?dset=fnmoc_obs_mcsst&summary=Go). TCHP data were from NOAA's Atlantic Oceanographic and Meteorological Laboratory (NOAA/AOML, available at https://www.aoml.noaa.gov/phod/cyclone/data/). SSS data were from NASA's Soil Moisture Active Passive (SMAP) sensor (available at https://smap.jpl.nasa.gov/). Chlorophyll-a data were from NASA's Moderate Resolution Imaging Spectroradiometer (MODIS) *Aqua* satellite (available at https://oceancolor.gsfc.nasa.gov/data/aqua/). SSH data were from the Copernicus Marine Environment Monitoring Service (available at: http://marine.copernicus.eu). Hurricane underwater glider data were from NOAA's Atlantic Oceanographic and Meteorological Laboratory (available at https://www.aoml.noaa.gov/phod/goos/gliders/index.php). Hurricane best track data are available from the National Hurricane Center (available at https://www.nhc.noaa.gov/data). Argo data were collected and made freely available by the International Argo Program and the national programs that contribute to it (available at http://www.argo.ucsd.edu, http://argo.jcommops.org). The aircraft observations of hurricane winds are archived by NOAA's Hurricane Research Division (HRD, available at http://www.aoml.noaa.gov/hrddata_sub/hurr.html). Model data are available upon request to the authors.

REFERENCES

Androulidakis, Y. S., V. H. Kourafalou, G. R. Halliwell Jr., M. Le Hénaff, H.-S. Kang, M. Mehari, and R. Atlas, 2016: Hurricane interaction with the upper ocean in the Amazon–Orinoco plume region. *Ocean Dyn.*, **66**, 1559–1588, https://doi.org/10.1007/s10236-016-0997-0.

Argo, 2020: Argo float data and metadata from global data assembly centre (Argo GDAC). SEANOE, https://doi.org/10.17882/42182.

Balaguru, K., P. Chang, R. Saravanan, L. R. Leung, Z. Xu, M. Li, and J.-S. Hsieh, 2012: Ocean barrier layers' effect on tropical cyclone intensification. *Proc. Natl. Acad. Sci. USA*, **109**, 14 343–14 347, https://doi.org/doi:10.1073/pnas.1201364109.

——, S. Taraphdar, L. R. Leung, G. R. Foltz, and J. A. Knaff, 2014: Cyclone–cyclone interactions through the ocean pathway. *Geophys. Res. Lett.*, **41**, 6855–6862, https://doi.org/10.1002/2014GL061489.

Berg, R., 2017: Hurricane Maria discussion number 6. National Hurricane Center, NOAA, accessed 22 August 2019, https://www.nhc.noaa.gov/archive/2017/al15/al152017.discus.006.shtml?

——, 2018: National Hurricane Center tropical cyclone report: Hurricane Jose (5–22 September 2017). NHC Tech. Rep. AL122017, 36 pp., https://www.nhc.noaa.gov/data/tcr/AL122017_Jose.pdf.

Bleck, R., 2002: An oceanic general circulation model framed in hybrid isopycnic-Cartesian coordinates. *Ocean Modell.*, **4**, 55–88, https://doi.org/10.1016/S1463-5003(01)00012-9.

Cangialosi, J. P., A. S. Latto, and R. Berg, 2018: National Hurricane Center tropical cyclone report: Hurricane Irma (30 August–12 September 2017). NHC Tech. Rep. AL112017, 111 pp., https://www.nhc.noaa.gov/data/tcr/AL112017_Irma.pdf.

Chen, H., and S. G. Gopalakrishnan, 2015: A study on the asymmetric rapid intensification of Hurricane Earl (2010) using the HWRF system. *J. Atmos. Sci.*, **72**, 531–550, https://doi.org/10.1175/JAS-D-14-0097.1.

Christophersen, H., A. Aksoy, J. Dunion, and S. Aberson, 2018: Composite impact of Global Hawk unmanned aircraft dropwindsondes on tropical cyclone analyses and forecasts. *Mon. Wea. Rev.*, **146**, 2297–2314, https://doi.org/10.1175/MWR-D-17-0304.1.

Cooper, M., and K. Haines, 1996: Altimetric assimilation with water property conservation. *J. Geophys. Res.*, **101**, 1059–1078, https://doi.org/10.1029/95JC02902.

Cucurull, L., and M. J. Mueller, 2020: An analysis of alternatives for the COSMIC-2 constellation in the context of Global Observing System Simulation experiments. *Wea. Forecasting*, **35**, 51–66, https://doi.org/10.1175/WAF-D-19-0185.1.

Cui, Z., Z. Pu, V. Tallapragada, R. Atlas, and C. S. Ruf, 2019: A preliminary impact study of CYGNSS ocean surface wind speeds on numerical simulations of hurricanes. *Geophys. Res. Lett.*, **46**, 2984–2992, https://doi.org/10.1029/2019GL082236.

Cummings, J. A., 2005: Operational multivariate ocean data assimilation. *Quart. J. Roy. Meteor.. Soc.*, **131**, 3583–3604, https://doi.org/10.1256/qj.05.105.

Dare, R. A., and J. L. McBride, 2011: Sea surface temperature response to tropical cyclones. *Mon. Wea. Rev.*, **139**, 3798–3808, https://doi.org/10.1175/MWR-D-10-05019.1.

Domingues, R., and Coauthors, 2015: Upper ocean response to Hurricane Gonzalo (2014): Salinity effects revealed by targeted and sustained underwater glider observations. *Geophys. Res. Lett.*, **42**, 7131–7138, https://doi.org/10.1002/2015GL065378.

——, G. Goni, M. Baringer, and D. Volkov, 2018: What caused the accelerated sea level changes along the U.S. East Coast during 2010–2015? *Geophys. Res. Lett.*, **45**, 13–367, https://doi.org/10.1029/2018GL081183.

——, and Coauthors, 2019: Ocean observations in support of studies and forecasts of tropical and extratropical cyclones. *Front. Mar. Sci.*, **6**, 446, https://doi.org/10.3389/fmars.2019.00446.

Dong, J., and Coauthors, 2017: Impact of assimilating underwater glider data on Hurricane Gonzalo (2014) forecasts. *Wea. Forecasting*, **32**, 1143–1159, https://doi.org/10.1175/WAF-D-16-0182.1.

Eriksen, C. C., T. J. Osse, R. D. Light, T. Wen, T. W. Lehman, P. L. Sabin, J. W. Ballard, and A. M. Chiodi, 2001: Seaglider: A long-range autonomous underwater vehicle for oceanographic research. *IEEE J. Oceanic Eng.*, **26**, 424–436, https://doi.org/10.1109/48.972073.

Ffield, A., 2007: Amazon and Orinoco River plumes and NBC rings: Bystanders or participants in hurricane events? *J. Climate*, **20**, 316–333, https://doi.org/10.1175/JCLI3985.1.

Fujii, Y., and Coauthors, 2019: Observing system evaluation based on ocean data assimilation and prediction systems: On-going challenges and future vision for designing/supporting ocean observational networks. *Front. Mar. Sci.*, **6**, 417, https://doi.org/10.3389/fmars.2019.00417.

Gallay, M. J. M., and Coauthors, 2019: Assessing Orinoco River sediment discharge trend using MODIS satellite images. *J. South Amer. Earth Sci.*, **91**, 320–331, https://doi.org/10.1016/j.jsames.2019.01.010.

Goes, J. I., and Coauthors, 2014: Influence of the Amazon River discharge on the biogeography of phytoplankton communities in the western tropical North Atlantic. *Prog. Oceanogr.*, **120**, 29–40, https://doi.org/10.1016/j.pocean.2013.07.010.

Goni, G. J., and W. E. Johns, 2001: A census of North Brazil Current rings observed from TOPEX/POSEIDON altimetry: 1992–1998. *Geophys. Res. Lett.*, **28**, 1–4, https://doi.org/10.1029/2000GL011717.

——, and R. Domingues, 2019: Tropical cyclones: Upper-ocean conditions in the Gulf of Mexico during Hurricane Michael [in ''State of the Climate in 2018'']. *Bull. Amer. Meteor. Soc.*, **100** (9), S135–S137, https://doi.org/10.1175/2019BAMSStateoftheClimate.1.

——, and Coauthors, 2009: Applications of satellite-derived ocean measurements to tropical cyclone intensity forecasting. *Oceanography*, **22**, 190–197, https://doi.org/10.5670/oceanog.2009.78.

——, and Coauthors, 2017: Autonomous and Lagrangian ocean observations for Atlantic tropical cyclone studies and forecasts. *Oceanography*, **30**, 92–103, https://doi.org/10.5670/oceanog.2017.227.

Good, S. A., G. K. Corlett, J. J. Remedios, E. J. Noyes, and D. T. Llewellyn-Jones, 2007: The global trend in sea surface temperature from 20 years of Advanced Very High Resolution Radiometer data. *J. Climate*, **20**, 1255–1264, https://doi.org/10.1175/JCLI4049.1.

Gopalakrishnan, S., F. Marks, X. Zhang, J.-W. Bao, K.-S. Yeh, and R. Atlas, 2011: The experimental HWRF system: A study on the influence of horizontal resolution on the structure and intensity changes in tropical cyclones using an idealized framework. *Mon. Wea. Rev.*, **139**, 1762–1784, https://doi.org/10.1175/2010MWR3535.1.

Gouveia, N. A., D. F. M. Gherardi, and L. E. O. C. Aragão, 2019: The role of the Amazon River plume on the intensification of the hydrological cycle. *Geophys. Res. Lett.*, **46**, 12 221–12 229, https://doi.org/10.1029/2019GL084302.

Halliwell, G. R., 2004: Evaluation of vertical coordinate and vertical mixing algorithms in the HYbrid-Coordinate Ocean Model (HYCOM). *Ocean Modell.*, **7**, 285–322, https://doi.org/10.1016/j.ocemod.2003.10.002.

——, L. K. Shay, S. D. Jacob, O. M. Smedstad, and E. W. Uhlhorn, 2008: Improving ocean model initialization for coupled tropical cyclone forecast models using GODAE nowcasts. *Mon. Wea. Rev.*, **136**, 2576–2591, https://doi.org/10.1175/2007MWR2154.1.

——, ——, J. K. Brewster, and W. J. Teague, 2011: Evaluation and sensitivity analysis of an ocean model response to Hurricane Ivan. *Mon. Wea. Rev.*, **139**, 921–945, https://doi.org/10.1175/2010MWR3104.1.

——, A. Srinivasan, V. H. Kourafalou, H. Yang, D. Willey, M. Le Hénaff, and R. Atlas, 2014: Rigorous evaluation of a fraternal twin ocean OSSE system for the open Gulf of Mexico. *J. Atmos. Oceanic Technol.*, **31**, 105–130, https://doi.org/10.1175/JTECH-D-13-00011.1.

——, S. Gopalakrishnan, F. Marks, and D. Willey, 2015: Idealized study of ocean impacts on tropical cyclone intensity forecasts. *Mon. Wea. Rev.*, **143**, 1142–1165, https://doi.org/10.1175/MWR-D-14-00022.1.

——, M. Mehari, M. Le Hénaff, V. H. Kourafalou, Y. S. Androulidakis, H.-S. Kang, and R. Atlas, 2017a: North Atlantic Ocean OSSE System: Evaluation of operational ocean observing system components and supplemental seasonal observations for potentially improving tropical cyclone prediction in coupled systems. *J. Oper. Oceanogr.*, **10**, 154–175, https://doi.org/10.1080/1755876X.2017.1322770.

——, ——, L. K. Shay, V. H. Kourafalou, H. Kang, H.-S. Kim, J. Dong, and R. Atlas, 2017b: OSSE quantitative assessment of rapid response prestorm ocean surveys to improve coupled tropical cyclone prediction. *J. Geophys. Res. Oceans*, **122**, 5729–5748, https://doi.org/10.1002/2017JC012760.

——, G. J. Goni, M. F. Mehari, V. H. Kourafalou, M. Baringer, and R. Atlas, 2020: OSSE assessment of underwater glider arrays to improve ocean model initialization for tropical cyclone prediction. *J. Atmos. Oceanic Technol.*, **37**, 467–487, https://doi.org/10.1175/JTECH-D-18-0195.1.

Hlywiak, J., and D. S. Nolan, 2019: The influence of oceanic barrier layers on tropical cyclone intensity as determined through idealized, coupled numerical simulations. *J. Phys. Oceanogr.*, **49**, 1723–1745, https://doi.org/10.1175/JPO-D-18-0267.1.

Hodges, J. L., 1958: The significance probability of the Smirnov two-sample test. *Ark. Mat.*, **3**, 469–486, https://doi.org/10.1007/BF02589501.

Kasahara, A., and G. W. Platzman, 1963: Interaction of a hurricane with the steering flow and its effect upon the hurricane trajectory. *Tellus*, **15**, 321–335, https://doi.org/10.3402/tellusa.v15i4.8863.

Kim, H.-S., C. Lozano, V. Tallapragada, D. Iredell, D. Sheinin, H. L. Tolman, V. M. Gerald, and J. Sims, 2014: Performance of ocean simulations in the coupled HWRF–HYCOM model. *J. Atmos. Oceanic Technol.*, **31**, 545–559, https://doi.org/10.1175/JTECH-D-13-00013.1.

Landsea, C. W., 1993: A climatology of intense (or major) Atlantic hurricanes. *Mon. Wea. Rev.*, **121**, 1703–1713, https://doi.org/10.1175/1520-0493(1993)121<1703:ACOIMA>2.0.CO;2.

——, 2017: Hurricane Irma discussion number 13. National Hurricane Center, NOAA, accessed 20 August 2019, https://www.nhc.noaa.gov/archive/2017/al11/al112017.discus.013.shtml.

Legler, D. M., and Coauthors, 2015: The current status of the real-time in-situ Global Ocean Observing System for operational oceanography. *J. Oper. Oceanogr.*, **8**, s189–s200, https://doi.org/10.1080/1755876X.2015.1049883.

Leipper, D. F., and D. Volgenau, 1972: Hurricane heat potential of the Gulf of Mexico. *J. Phys. Oceanogr.*, **2**, 218–224, https://doi.org/10.1175/1520-0485(1972)002<0218:HHPOTG>2.0.CO;2.

Locarnini, R. A., and Coauthors, 2013: *Temperature*. Vol. 1, *World Ocean Atlas 2013*, NOAA Atlas NESDIS 73, 48 pp., http://data.nodc.noaa.gov/woa/WOA13/DOC/woa13_vol1.pdf.

Lueck, R. G., and J. J. Picklo, 1990: Thermal inertia of conductivity cells: Observations with a Sea-Bird cell. *J. Atmos. Oceanic Technol.*, **7**, 756–768, https://doi.org/10.1175/1520-0426(1990)007<0756:TIOCCO>2.0.CO;2.

Mainelli, M., M. DeMaria, L. K. Shay, and G. Goni, 2008: Application of oceanic heat content estimation to operational forecasting of recent Atlantic category-5 hurricanes. *Wea. Forecasting*, **23**, 3–16, https://doi.org/10.1175/2007WAF2006111.1.

Miles, T., G. Seroka, J. Kohut, O. Schofield, and S. Glenn, 2015: Glider observations and modeling of sediment transport in Hurricane Sandy. *J. Geophys. Res. Oceans*, **120**, 1771–1791, https://doi.org/10.1002/2014JC010474.

Mogensen, K. S., L. Magnusson, and J. R. Bidlot, 2017: Tropical cyclone sensitivity to ocean coupling in the ECMWF coupled model. *J. Geophys. Res. Oceans*, **122**, 4392–4412, https://doi.org/10.1002/2017JC012753.

Morison, J., R. Andersen, N. Larson, E. D'Asaro, and T. Boyd, 1994: The correction for thermal-lag effects in Sea-Bird CTD data. *J. Atmos. Oceanic Technol.*, **11**, 1151–1164, https://doi.org/10.1175/1520-0426(1994)011<1151:TCFTLE>2.0.CO;2.

Murakami, H., E. Levin, T. L. Delworth, R. Gudgel, and P. C. Hsu, 2018: Dominant effect of relative tropical Atlantic warming on major hurricane occurrence. *Science*, **362**, 794–799, https://doi.org/10.1126/science.aat6711.

National Hurricane Center, 2017: Monthly tropical weather summary, December 2017. National Hurricane Center, accessed 7 January 2020, https://www.nhc.noaa.gov/archive/text/TWSAT/2017/TWSAT.201712011244.txt.

Oke, P. R., and Coauthors, 2009: Observing System Evaluations: Using GODAE Systems. *Oceanography*, **22**, 144–153, https://doi.org/10.5670/oceanog.2009.72.

——, and Coauthors, 2015: Assessing the impact of observations on ocean forecasts and reanalyses: Part 1, Global studies. *J. Oper. Oceanogr.*, **8**, s49–s62, https://doi.org/10.1080/1755876X.2015.1022067.

Pasch, R. J., A. B. Penny, and R. Berg, 2019: National Hurricane Center tropical cyclone report: Hurricane Maria (16–30 September 2017). NHC Tech. Rep. AL152017, 48 pp., https://www.nhc.noaa.gov/data/tcr/AL152017_Maria.pdf.

Polyakov, I. V., V. A. Alexeev, U. S. Bhatt, E. I. Polyakova, and X. Zhang, 2010: North Atlantic warming: Patterns of long-term trend and multidecadal variability. *Climate Dyn.*, **34**, 439–457, https://doi.org/10.1007/s00382-008-0522-3.

Reul, N., Y. Quilfen, B. Chapron, S. Fournier, V. Kudryavtsev, and R. Sabia, 2014a: Multisensor observations of the Amazon–Orinoco River plume interactions with hurricanes. *J. Geophys. Res. Oceans*, **119**, 8271–8295, https://doi.org/10.1002/2014JC010107.

——, and Coauthors, 2014b: Sea surface salinity observations from space with the SMOS satellite: A new means to monitor the marine branch of the water cycle. *Surv. Geophys.*, **35**, 681–722, https://doi.org/10.1007/s10712-013-9244-0.

Reynolds, R. W., N. A. Rayner, T. M. Smith, D. C. Stokes, and W. Wang, 2002: An improved in situ and satellite SST analysis for climate. *J. Climate*, **15**, 1609–1625, https://doi.org/10.1175/1520-0442(2002)015<1609:AIISAS>2.0.CO;2.

Rudzin, J. E., L. K. Shay, and W. E. Johns, 2018: The influence of the barrier layer on SST response during tropical cyclone wind forcing using idealized experiments. *J. Phys. Oceanogr.*, **48**, 1471–1478, https://doi.org/10.1175/JPO-D-17-0279.1.

——, ——, and B. Jaimes de la Cruz, 2019: The impact of the Amazon–Orinoco River plume on enthalpy flux and air–sea interaction within Caribbean Sea tropical cyclones. *Mon. Wea. Rev.*, **147**, 931–950, https://doi.org/10.1175/MWR-D-18-0295.1.

Santos-Burgoa, C., and Coauthors, 2018: Ascertainment of the estimated excess mortality from Hurricane Maria in Puerto Rico. Milken Institute School of Public Health, George Washington University, 69 pp., https://www.washingtonblade.com/content/files/2018/09/PuertoRicoReport.pdf.

Schott, T., and Coauthors, 2019: The Saffir–Simpson Hurricane wind scale. National Hurricane Center, NOAA, 4 pp., https://www.nhc.noaa.gov/pdf/sshws.pdf.

Seroka, G., T. Miles, Y. Xu, J. Kohut, O. Schofield, and S. Glenn, 2017: Rapid shelf-wide cooling response of a stratified coastal ocean to hurricanes. *J. Geophys. Res. Oceans*, **122**, 4845–4867, https://doi.org/10.1002/2017JC012756.

Shapiro, L. J., 1982: Hurricane climatic fluctuations. Part II: Relation to large-scale circulation. *Mon. Wea. Rev.*, **110**, 1014–1023, https://doi.org/10.1175/1520-0493(1982)110<1014:HCFPIR>2.0.CO;2.

Shay, L. K., and S. D. Jacob, 2006: Relationship between oceanic energy fluxes and surface winds during tropical cyclone passage. *Atmosphere Ocean Interactions II: Advances in Fluid Mechanics*, W. Perrie, Ed., WIT Press, 115–142.

——, and E. W. Uhlhorn, 2008: Loop Current response to hurricanes Isidore and Lili. *Mon. Wea. Rev.*, **136**, 3248–3274, https://doi.org/10.1175/2007MWR2169.1.

——, G. J. Goni, and P. G. Black, 2000: Effects of a warm oceanic feature on Hurricane Opal. *Mon. Wea. Rev.*, **128**, 1366–1383, https://doi.org/10.1175/1520-0493(2000)128<1366:EOAWOF>2.0.CO;2.

Smith, R. K., J. A. Zhang, and M. T. Montgomery, 2017: The dynamics of intensification in a Hurricane Weather Research and Forecasting simulation of Hurricane Earl (2010). *Quart. J. Roy. Meteor. Soc.*, **143**, 293–308, https://doi.org/10.1002/qj.2922.

Smith, W. O., Jr., and D. J. Demaster, 1996: Phytoplankton biomass and productivity in the Amazon River plume: Correlation with seasonal river discharge. *Cont. Shelf Res.*, **16**, 291–319, https://doi.org/10.1016/0278-4343(95)00007-N.

Tallapragada, V., C. Kieu, Y. Kwon, S. Trahan, Q. Liu, Z. Zhang, and I. H. Kwon, 2014: Evaluation of storm structure from the operational HWRF during 2012 implementation. *Mon. Wea. Rev.*, **142**, 4308–4325, https://doi.org/10.1175/MWR-D-13-00010.1.

Vissa, N. K., A. N. V. Satyanarayana, and B. P. Kumar, 2013: Response of upper ocean and impact of barrier layer on Sidr cyclone induced sea surface cooling. *Ocean Sci. J.*, **48**, 279–288, https://doi.org/10.1007/s12601-013-0026-x.

Volkov, D. L., S. K. Lee, R. Domingues, H. Zhang, and M. Goes, 2019: Interannual sea level variability along the southeastern seaboard of the United States in relation to the gyre-scale heat divergence in the North Atlantic. *Geophys. Res. Lett.*, **46**, 7481–7490, https://doi.org/10.1029/2019GL083596.

Wang, X., G. Han, Y. Qi, and W. Li, 2011: Impact of barrier layer on typhoon-induced sea surface cooling. *Dyn. Atmos. Oceans*, **52**, 367–385, https://doi.org/10.1016/j.dynatmoce.2011.05.002.

Zhang, J. A., D. S. Nolan, R. F. Rogers, and V. Tallapragada, 2015: Evaluating the impact of improvements in the boundary layer parameterizations on hurricane intensity and structure forecasts in HWRF. *Mon. Wea. Rev.*, **143**, 3136–3155, https://doi.org/10.1175/MWR-D-14-00339.1.

Zou, X., F. Weng, B. Zhang, L. Lin, Z. Qin, and V. Tallapragada, 2013: Impacts of assimilation of ATMS data in HWRF on track and intensity forecasts of 2012 four landfall hurricanes. *J. Geophys. Res. Atmos.*, **118**, 11 558–11 576, https://doi.org/10.1002/2013JD020405.

Zweng, M. M., and Coauthors, 2013: *Salinity*. Vol. 2, *World Ocean Atlas 2013*, NOAA Atlas NESDIS 74, 39 pp., http://data.nodc.noaa.gov/woa/WOA13/DOC/woa13_vol2.pdf.